RESEARCH ARTICLE

Adult spinal Dmrt3 neurons receive direct somatosensory inputs from ipsi- and contralateral primary afferents and from brainstem motor nuclei

Jennifer Vieillard[1],* | Marina C. M. Franck[1,2],* | Sunniva Hartung[1] |
Jon E. T. Jakobsson[1] | Mikaela M. Ceder[1] | Robert E. Welsh[1] |
Malin C. Lagerström[1],# | Klas Kullander[1],#

[1]Department of Immunology, Genetics and Pathology, Uppsala University, Uppsala, Sweden

[2]Present address: Department of Medical Biochemistry and Biophysics, Karolinska Institutet, Stockholm, Sweden

Correspondence
Klas Kullander and Malin C. Lagerström, Department of Immunology, Genetics and Pathology, Uppsala University, 751 08 Uppsala, Sweden.
Email: klas.kullander@igp.uu.se, malin.lagerstrom@igp.uu.se

*Jennifer Vieillard and Marina C. M. Franck contributed equally to this article.
#Malin C. Lagerström and Klas Kullander contributed equally to this article.

Abstract

In the spinal cord, sensory-motor circuits controlling motor activity are situated in the dorso–ventral interface. The neurons identified by the expression of the transcription factor Doublesex and mab-3 related transcription factor 3 (Dmrt3) have previously been associated with the coordination of locomotion in horses (*Equus caballus*, Linnaeus, 1758), mice (*Mus musculus*, Linnaeus, 1758), and zebrafish (*Danio rerio*, F. Hamilton, 1822). Based on earlier studies, we hypothesized that, in mice, these neurons may be positioned to receive sensory and central inputs to relay processed commands to motor neurons. Thus, we investigated the presynaptic inputs to spinal Dmrt3 neurons using monosynaptic retrograde replication-deficient rabies tracing. The analysis showed that lumbar Dmrt3 neurons receive inputs from intrasegmental neurons, and intersegmental neurons from the cervical, thoracic, and sacral segments. Some of these neurons belong to the excitatory V2a interneurons and to plausible Renshaw cells, defined by the expression of Chx10 and calbindin, respectively. We also found that proprioceptive primary sensory neurons of type Ia2, Ia3, and Ib, defined by the expression of calbindin, calretinin, and Brn3c, respectively, provide presynaptic inputs to spinal Dmrt3 neurons. In addition, we demonstrated that Dmrt3 neurons receive inputs from brain areas involved in motor regulation, including the red nucleus, primary sensory–motor cortex, and pontine nuclei. In conclusion, adult spinal Dmrt3 neurons receive inputs from motor-related brain areas as well as proprioceptive primary sensory neurons and have been shown to connect directly to motor neurons. Dmrt3 neurons are thus positioned to provide sensory–motor control and their connectivity is suggestive of the classical reflex pathways present in the spinal cord.

1 | INTRODUCTION

To sense and move are functions required for animals to perform essential behaviors such as escaping predators and finding shelter and food. In spinal cord networks, sensory information is gated to motor command circuits, as well as being forwarded to the brain for emotional, cognitive, and conscious processing. Such centrally processed commands are relayed back to the spinal cord for additional autonomous and voluntary control of motor behaviors. Excitatory and inhibitory interneurons in the spinal cord serve as an interface between sensory inputs and motor commands, and provide entry points for the congregation of direct and processed information to achieve the most purposeful movement at any given moment (Akay & Murray, 2021; Goulding et al., 2014; Grillner, 2021; Stachowski & Dougherty, 2021). The identity and connectivity of specified interneuron populations is therefore required to disentangle the neuronal circuits of the spinal cord that control and modulate sensorimotor function.

Ten gross populations of interneurons in the spinal cord termed dI1 to dI6 (dorsal interneuron class 1 to 6) and V0 to V3 (ventral interneuron class 0 to 3) are derived from progenitor domains, which are grouped by their expression of transcription factors during embryogenesis (Lu et al., 2015). This basic division of interneurons have greatly aided in the efforts to assign function to neurons, and most of the dorsal populations in the spinal cord have been related to sensory function, whereas ventral populations are more related to motor function (Stachowski & Dougherty, 2021). One exception is the dI6 population, containing neurons expressing the Doublesex and mab-3 related transcription factor 3 (Dmrt3), since they arise from the dorsal progenitor domain 6, but migrate ventrally during development and are involved in regulating locomotion and gait coordination (Andersson et al., 2012; Del Pozo et al., 2020; Satou et al., 2020). Indeed, a genomic investigation of Icelandic horses has revealed that homozygosity for a *DMRT3* nonsense mutation is permissive for alternative gaits, such as toelt and flying pace (Andersson et al., 2012). Further, neonatal *Dmrt3*-null mice display uncoordinated hindlimb movements during air-stepping and are almost completely unable to perform left–right alternation of their hindlimbs. *Dmrt3*-null adult mice have milder gait coordination abnormalities including difficulties at running at high speed and increased stride duration. The data collected so far, thus suggest that correct expression of the transcription factor Dmrt3 is required for proper assembly of a functional locomotor central pattern generator (CPG) during development (Andersson et al., 2012; Del Pozo et al., 2020; Satou et al., 2020).

In mice, Dmrt3-expressing spinal interneurons are inhibitory and mainly commissural (Iglesias González et al., 2021; Perry et al., 2019). The role of these neurons in locomotor circuits, together with previous findings indicating that the population has a direct connection to motor neurons and a fast response to dorsal root stimulation, suggests an involvement in spinal sensorimotor reflex circuits (Perry et al., 2019). However, the role of Dmrt3 interneurons in awake behaving animal is still unresolved. The position of this dI6 population at the interface between the ventral and dorsal spinal cord may also indicate a role for the Dmrt3 population

in sensory–motor integration. The corticospinal tract originates in the motor and somatosensory cortices and, together with descending tracts from the brainstem, regulates the activity in spinal sensory and motor circuits (Ueno et al., 2018). These spinal sensory–motor circuits also receive sensory input from dorsal root ganglia neurons, which influence circuit activity through mechanosensory and proprioceptive inputs.

To probe the hypothesis that adult spinal Dmrt3 neurons may integrate sensory and motor inputs, we used monosynaptic retrograde tracing combined with immunolabeling to carefully characterize the type of inputs that are received by the Dmrt3 neurons. We found cells monosynaptically connected to spinal Dmrt3 neurons in brain regions known to project to the lumbar spinal cord, including the neocortex, the midbrain red nucleus, the pontine reticular nucleus, the medullary gigantocellular reticular nucleus, and vestibular nuclei. We also found a large number of monosynaptically connected cells in the spinal cord at all levels, and in both ipsi- and contralateral DRG of proprioceptor sub-type, clearly positioning adult Dmrt3 neurons in a position for sensorimotor integration. Of note, this study focused on mature circuits and revealed a position of adult Dmrt3 inhibitory interneurons in the circuits of proprioception, immediately downstream of Ia and Ib primary afferents.

2 | MATERIALS AND METHODS

2.1 | Animals

All animal procedures were approved by the local animal research ethical committee (Uppsala djurförsöksetiska nämnd) and followed the Swedish Animal Welfare Act (Svensk författningssamling [SFS] 2018:1192), The Swedish Animal Welfare Ordinance (SFS 2019:66) and the Regulations and general advice for laboratory animals (SJVFS 2019:9, Saknr L 150). Ethical permit number: 5.8.18-08463/2018. Both female and male mice were used. Dmrt3-Cre mice (RRID:IMSR_EM:13798, Perry et al., 2019) were crossed with either C57BL/6(Taconic) or *GT(ROSA)26Sortm14(CAG-tdTomato)Hze* mice (Allen Brain Institute RRID: IMSR_JAX:007914; Madisen et al., 2010), and the offspring were genotyped in house for the presence of the Dmrt3-Cre allele and/or the tdTomato allele. The following primers were used: Dmrt3-Cre 5′-gagactgctgccgtagctccg3′ (forward), and 5′-cttcatcagaggtggcatccacag-3′ (reverse); tdTomato 5′-ctgttcctgtacggcatgg-3′ (forward), 5′-ggcattaaagcagcgtatcc-3′ (reverse). The Dmrt3-Cre allele was kept heterozygous.

2.2 | Viral injections

Five Dmrt3-Cre mice and five Cre-negative animals (four littermates of the Cre-positive animals and one C57BL/6) were used for viral injections of helper viruses and the EnvA-ΔG-mCherry rabies virus (for age and sex see Table 1). Animals were first injected with a helper virus mix (1 or 2 injections of 475 nl of

TABLE 1 Experimental design. Summary of the number of Dmrt3-Cre+ and control animals, including their sex, age, number and coordinates of injections, the number of incubation days after injections, the location of the estimated starter cells, and the percentage of them located in the contralateral side

Mice	Sex	Age in months	Number of helper virus injection	Number of rabies virus injection	Injection side and coordinates	Days of virus incubation	Location of estimated starter cells	Percentage of contralateral estimated starter cells
Cre+ 1	f	5	2 (1 mm apart)	2 (2 mm apart)	Left 0.4 mm lateral 0.9 mm down	5 + 8	L5 and L6	0%
Cre+ 2	f	5	2 (2 mm apart)	1	Left 0.3 mm lateral 0.9 mm down	7 + 7	S1	Around 10%
Cre+ 3	f	2	1	1	Right 0.5 mm lateral 0.9 mm down	5 + 8	L5	0%
Cre+ 4	f	3	1	1	Right 0.5 mm lateral 0.9 mm down	6 + 7	L5	Not analysed, very few estimated starter cells
Cre+ 5	m	4	2 (0.8 mm apart)	1	Right 0.4 mm lateral 0.9 mm down	7 + 7	L5	0%
Control 1 Cre-	f	5	2 (1 mm apart)	2 (2 mm apart)	Left 0.3 mm lateral 0.9 mm down	7 + 7	Table 4	0%
Control 2 Cre-	f	3	1	1	Right 0.5 mm lateral 0.9 mm down	5 + 8	Table 4	0%
Control 3 Cre-	f	3	1	1	Right 0.5 mm lateral 0.9 mm down	6 + 7	Table 4	0%
Control 4 Cre-	m	4	2 (0.8 mm apart)	1	Right 0.4 mm lateral 0.9 mm down	7 + 7	Table 4	0%
Control 5 C57Bl/6	f	1,5	2 (0.8 mm apart)	1	Right 0.4 mm lateral 0.9 mm down	7 + 7	Table 4	0%

AAV2-EF1a-FLEX-GFP-TVA, titer: 4.44×10^{11} vg/ml(Addgene plasmid # 26198; http://n2t.net/addgene:26198; RRID:Addgene_26198) (Wall et al., 2010) and 25 nl of AAV9-CAG-FLEX-oG-WPRE-SV40-pA (titer: 1.78×10^{11} vg/ml, Addgene plasmid # 74292; http://n2t.net/addgene:74292; RRID:Addgene_74292) (Kim et al., 2016) and 5 to 7 days later with the EnvA-ΔG-mCherry rabies virus (Addgene plasmid # 32636; http://n2t.net/addgene:32636; RRID:Addgene_32636) (Osakada et al., 2011) (1 or 2 injections of 500 nl EnvA-ΔG-mCherry rabies virus). All these viruses were purchased from Salk Institute, originally a gift from Edward Callaway. Seven to 8 days after the last surgery, the animals were perfused for tissue analysis. Dmrt3-Cre/tdTomato animals ($n = 3$, females, age 8 months) were only injected with AAV2-EF1a-FLEX-GFP-TVA virus and perfused 2 weeks later. Animals ($n = 2$ females, 4–5 months old) for MAP2 immunohistochemistry were injected unilaterally with 500 nl of AAV8-hSyn-DIO-hM3dq-mCherry (titer 2.0×10^{13}, purchased from Addgene, originally a gift from Bryan Roth, Addgene viral prep # 44361-AAV8; http://n2t.net/addgene:44361; RRID:Addgene_44361) (Krashes et al., 2011).

The animals were anesthetized with isoflurane (Baxter, induction at 4% and then continuous anesthesia at 2%, isoflurane with air 0.5–2 L/min), and the body temperature was monitored and maintained at 36–37°C during the procedure using a heating pad (CMA, Sweden). The fur on the back was shaved, the skin disinfected with chlorhexidine (Fresenius Kabi, Sweden), and a 1–2 cm incision was made along the midline above vertebrae T13–L1, followed by a second incision through the connective tissue covering these two vertebrae to access spinal cord segments L4–L5. Next, a clamp was inserted around vertebra L1 to secure the spinal column. The ligaments connecting T13 with L1 were cut to reveal the spinal cord. One or two (0.8–2 mm apart) unilateral injections of 500 nl virus each were made into the spinal cord parenchyma 0.3–0.5 mm lateral of the midline and 0.9 mm ventral of the spinal cord surface using a 10 μl Nanofil Hamilton syringe (WPI, USA) with a 34G beveled needle (WPI, USA) guided by a microsyringe pump controller (WPI, USA) mounted on a stereotaxic frame. The tissue was kept moist throughout the procedure by continuous application of sterile saline (9 mg/ml, Fresenius Kabi, Sweden) on the surgical area. Bupivacaine (Marcain; AstraZeneca, 2 mg/kg)

TABLE 2 List of primary antibodies

Primary antibody	Supplier	Concentration
Chicken anti-GFP	Aves Labs (GFP-1020)	1/1000
Mouse anti-calretinin	Swant (6B3)	1/500
Rabbit anti-PKCγ	Santa Cruz (sc-211)	1/500
Rabbit anti-Parvalbumin	Swant (PV27)	1/1000
Rabbit anti-Calretinin	Swant (7697)	1/500
Rabbit anti-Calbindin	Swant (CB38)	1/1000
Mouse anti-Brn3c	Santa cruz (sc-81980)	1/200
Rat anti-mCherry	ThermoFisherScientific (16D7)	1/500
Rabbit anti-CGRP	Peninsula Laboratories (T-4239)	1/500
Rabbit anti-NF200	Sigma (N4142)	1/1000
Sheep anti-Chx10	Exalpha (X1180P)	1/300
Rabbit anti-TH	Millipore (AB152)	1/1000
Goat anti-ChAT	Millipore (AB144P)	1/100
Rabbit anti-MAP2	Millipore (AB5622)	1/1000

TABLE 3 List of secondary antibodies

Secondary antibody and isolectin	Supplier	Concentration
Donkey anti-rabbit A488	ThermoFisherScientific A32790	1/1000
Donkey anti-rabbit A647	ThermoFisherScientific A32795	1/1000
Donkey anti-mouse A647	ThermoFisherScientific A-31571	1/500
Goat anti-chicken A488	Jackson ImmunoResearch 103-545-155	1/1000
Donkey anti-sheep A647	ThermoFisherScientific A-21448	1/500
Donkey anti-rat A598	ThermoFisherScientific A-21209	1/1000
Isolectin GS-IB4 AlexaFluor 647 conjugate	ThermoFisherScientific (I32450)	1/1000

was administered as a local anesthetic at the site of surgery and karprofen (Norocarp vet; N-vet, 5 mg/kg) was used for postoperative analgesia.

2.3 | Tissue preparation and immunohistochemistry

To fix the tissue for immunohistochemical analysis, the mice were transcardially perfused with PBS (ThermoFisher, Sweden) followed by 4% formaldehyde (Histolab, Sweden) in PBS. The spinal cords, dorsal root ganglia (DRG), and brains were dissected out and post-fixed in 4% formaldehyde overnight at 4°C and then washed 3 times in PBS. Tissues for vibratome sectioning were embedded in 4% agarose and the spinal cord sectioned at 50–60 μm (one Dmrt3-Cre animal and all the controls) and the brains sectioned at 60–100 μm (all the animals). Tissues for cryosectioning were incubated in a sequence of 10%, 20%, and 30% sucrose in PBS. The tissue was mounted in cryostat embedding medium (Killik Bio-Optica, Italy) and snap frozen in dry ice cooled isopentane (Sigma). Sections were cut using a Cryocut 1800 cryostat (Leica, Germany). Spinal cords were sectioned at 20 μm and DRG between 7 μm and 12 μm, and the sections were stored at −20°C until used.

For immunohistochemical analysis of frozen sections, slides were thawed and dried for 30 to 45 min, and then washed in PBS three times for 10 min. Sections were blocked for 1 h in blocking solution (5% donkey serum [VWR], 3% BSA [Sigma], 0.3% Triton X-100 [Sigma] in PBS) at room temperature. Primary antibodies (see Antibody characterization section and Table 2 for details) were incubated on the slides for approximately 16 h at 4°C (or 48 h for Brn3c). Sections were washed three times for 15 min in PBS and then incubated with secondary antibodies

and for some DRG sections with isolectin GS-IB4 AlexaFluor647 conjugate (see Table 3 for details) mixed in blocking solution (with DAPI 200 ng/ml) for 1 h. Sections were washed three times for 15 min in PBS, and then mounted in ProLong® Gold Antifade Mountant (Life Technologies, USA) or Fluoroshield (Abcam, UK). For MAP2 immunohistochemistry, the lumbar spinal cord was sectioned at 40 μm with the vibratome, and the staining was performed on free-floating sections as described above. The only difference is the blocking buffer (5% donkey serum (VWR), 3% BSA (Sigma), 0.5% Triton X-100 (Sigma) in PBS) and the 48 h primary antibody incubation.

2.4 | Antibody characterization

The list of the antibodies used in this study is recapitulated in Table 2.

2.4.1 | Anti-GFP

The polyclonal green fluorescent protein (GFP) antibody made in chicken (Aves Labs Cat# GFP-1020, RRID:AB_10000240, used at 1:1000) was produced by immunizing chickens with a purified recombinant GFP. The specificity of the antibody was verified by Western blot and immunostaining on transgenic mouse expressing GFP (manufacturer datasheet).

2.4.2 | Anti-calretinin

The monoclonal calretinin antibody (Swant Cat# 6B3, RRID:AB _10000320, used at 1:500) was made by immunization of mice with a recombinant human calretinin-22k. It recognized a 29 kDa band on immunoblot performed on brain extracts from different animal species (including rats and mice) and immunohistochemistry performed with

this antibody on brains from control and calretinin knock-out mice showed its specificity (manufacturer datasheet).

The polyclonal calretinin serum (Swant Cat# CR 7697, RRID:AB _2619710, used at 1:500) was produced by immunization of rabbits with a recombinant human calretinin containing a 6-his tag at the N-terminal. In Western blot on brain from different species (among which mice), the antiserum specifically recognizes a band of 29–30 kDa, and immunohistochemistry performed with this antibody on brains from control and calretinin knock-out mice showed its specificity (manufacturer datasheet).

2.4.3 | Anti-PKCγ

The PKCγ (C-19) antibody (Santa Cruz Biotechnology Cat# sc-211, RRID:AB_632234, used at 1:500) is a polyclonal rabbit antibody that recognizes a peptide mapping at the C-terminus of the mouse PKCγ protein. Western blot performed on 293T cell lysates transfected with human PKCγ showed a band between 69 kDa and 101 kDa (manufacturer datasheet). No PKCγ staining was observed in the brain and spinal cord of PKCγ knock-out mice (Malmberg et al., 1997).

2.4.4 | Anti-parvalbumin

The polyclonal parvalbumin rabbit antiserum (Swant Cat# PV27, RRID:AB_2631173, used at 1:1000) recognizes the recombinant rat parvalbumin protein. Western blot performed on brain extract from wildtype mouse shows a band of 12 kDa, which is absent in brain extracts from parvalbumin knock-out mice. Immunostainings with PV27 performed on hippocampus from parvalbumin knock-out mice demonstrated the specificity of this antiserum (manufacturer datasheet).

2.4.5 | Anti-calbindin

The rabbit anti-Calbindin D-28k antiserum (Swant Cat# CB38, RRID:AB_10000340, used at 1:1000) was raised against a recombinant rat calbindin D−28k. Western blot performed on brain lysates from different species showed a band of 28 kDa. Immunostainings with CB38 performed on cerebellum from calbindin knock-out mice demonstrated the specificity of this antiserum (manufacturer datasheet).

2.4.6 | Anti-Brn3c

The mouse monoclonal IgG1 anti-Brn3c antibody (Santa Cruz Biotechnology Cat# sc-81980, RRID:AB_2167543, used at 1:200) was raised against recombinant human Brn3c protein. Western blot performed on nuclear lysates from HeLa cells showed a band between 25 kDa and 37 kDa (manufacturer datasheet).

2.4.7 | Anti-mCherry

The monoclonal IgG2 rat antibody (Thermo Fisher Scientific Cat# M11217, RRID:AB_2536611, used at 1:500) was raised against the full-length protein mCherry. Western blot performed on lysates from HEK-293 cells transfected with a mCherry-histone H3 construct showed a band of 43 kDa and the weight of H3-mCherry. No band was detected in the lysates from untransfected cells. Immunostaining with 1D7 on HEK-293 cells transfected with a mCherry-histone H3 construct showed nuclear expression. There was no staining in untransfected cells.

2.4.8 | Anti-CGRP

The polyclonal CGRP antiserum (Peninsula Laboratories Cat# T-4239.0050, RRID:AB_518150, used at 1:500) was made by immunization of rabbits with a synthetic peptide from human protein. Immunostaining performed with this antibody showed the expression of CGRP in spinal cord dorsal horn from wildtype mice. No expression was observed in α-CGRP knock-out mice (Gangula et al., 2000). Western blot performed on spinal cord and DRG lysates using this antiserum showed a band (Wang et al., 2011).

2.4.9 | Anti-NF200

The polyclonal NF200 rabbit antibody (Sigma-Aldrich Cat# N4142, RRID:AB_477272, used at 1:1000) was raised against the Neurofilament200 protein from bovine spinal cord. Western blot performed with NF200 antibody on lysates from wildtype mice optic nerves, corpus callosum, spinal cord, and sciatic nerves showed a band which was absent in the same tissue from α-internexin, neurofilament heavy polypeptide (NFH), and neurofilament light polypeptide (NFL) triple knockout mice (Yuan et al., 2015).

2.4.10 | Anti-Chx10

The sheep polyclonal Chx10 antibody (Exalpha Cat# X1180P, RRID:AB _2314191, used at 1:300) was raised against a recombinant protein corresponding to amino acids 1 to 131 derived from the N-terminal region of the human Chx10 protein. Western blot performed with this antibody in retina lysates from mice and rats showed a band around 50 kDa when there was no band in lysates from liver tissue (manufacturer datasheet).

2.4.11 | Anti-TH

The purified anti-TH rabbit polyclonal antibody (Millipore Cat# AB152, RRID:AB_390204, used at 1:1000) was raised against the denatured

tyrosine hydroxylase protein from rat pheochromocytoma. Western blot performed on lysates from PC12 cells showed a band around 62 kDa (manufacturer datasheet). In mouse brain, immunostaining using this anti-TH antibody showed expression of TH in the locus coeruleus. In conditional TH-flox mutant in DbhCre-positive neurons, there was no staining of TH in the locus coeruleus (Tsetsenis et al., 2021).

2.4.12 | Anti-ChAT

The purified anti-ChAT goat polyclonal antibody (Millipore Cat# AB144P, RRID:AB_2079751, used at 1:100) was raised against Human placental enzyme. Western blot performed on NIH/3T3 cell lysates with this antibody showed a band around 68–70 kDa (manufacturer datasheet). Immunohistochemistry performed on mouse embryo spinal cords with this antibody showed motor neuron staining in the ventral horn which was absent from ChAT knock-out mice (Misgeld et al., 2002).

2.4.13 | Anti-MAP2

The purified anti-MAP2 rabbit antibody (Millipore Cat# AB5622, RRID:AB_91939, used at 1:1000) was raised against purified microtubule-associated protein from rat brain. Western blot performed on rat brain extracts showed a single band (manufacturer datasheet). Immunohistochemistry performed with this antibody on cultured hippocampal neurons from mice showed the expression of MAP2 in the dendrites of the neurons as expected (Bodaleo et al., 2016).

2.5 | Imaging and post processing

Wide field images were taken using an Olympus BX61WI fluorescence microscope (Olympus, Japan) with a Volocity software (Quorum Technologies) or a Zeiss Axio Imager Z2 (Zeiss, Germany) with a colibri LED 7 and Zen blue software (Zeiss, Germany). Some images were taken using a Zeiss LSM700 confocal microscope (BioVis facility, Uppsala University). Brightness and contrast were adjusted in ImageJ, equally for the whole image and without obscuring any data. Images of brainstem were stitched using the Pairwise Stitching in ImageJ (ImageJ, RRID:SCR_003070) (Preibisch et al., 2009). Cell counts were done manually with ImageJ's Cell counter plugin (Schneider et al., 2012). For estimation of the total number of traced cells in the spinal cord, cells were identified and counted using an ImageJ macro based on signal intensity and size. A selection of automatically counted images was re-counted manually, and the macro was found to identify 50–80% of cells.

Brain regions were identified based on the Allen Brain atlas and The Mouse Brain in Stereotaxic Coordinates (MBSC) (Franklin & Paxinos, 2008; Lein et al., 2007). Abbreviations followed the MBSC.

3 | RESULTS

3.1 | Rabies monosynaptic tracing is a valid method for exploring the connectivity of ventral spinal cord interneurons

In this study, the aim was to identify the pre-synaptic neurons projecting onto lumbar Dmrt3-expressing interneurons using a rabies virus-based approach (Figure 1a). Here, an EnvA-ΔG-mCherry rabies virus was used, which requires a TVA receptor (avian tumor virus receptor A) to enter cells, and an oG protein (optimized glycoprotein for rabies virus SAD B19) to retrogradely cross a synapse (Figure 1b). The TVA and oG proteins, together with GFP, are dependent on the Cre-protein for their expression and are delivered into the spinal cord by two adeno-associated virus (AAV) helper viruses. With the introduction and rise of this technique, undesired leakage of the TVA receptor expression has been reported, which can lead to unspecific rabies virus expression and unreliable results (Lavin et al., 2020). Moreover, retrograde tracing experiments have not yet, to our knowledge, been performed on interneurons located in the ventral spinal cord. Hence, control experiments were first carried out to verify that the rabies virus-based technique is suitable to study presynaptic connections onto ventral spinal cord interneurons.

First, the specificity of the AAV2-EF1a-FLEX-GFP-T2A-TVA (hereafter referred to as TVA-GFP) helper virus was evaluated by injection into the lumbar spinal cord of Dmrt3-Cre/tdTomato reporter animals (Figure 1c–e). Nearly all cells expressing GFP also expressed tdTomato (tdTomato expression was found in 98.5% of GFP-expressing cells [603 out of 612 GFP-expressing cells] $n = 3$ animals), indicating that the GFP and TVA proteins were strongly expressed in the Cre-expressing Dmrt3 neurons in lamina VII and VIII, and that Cre activity in these cells persists into adulthood, even though the expression of *Dmrt3* mRNA has been shown to decrease after birth (Perry et al., 2019).

Next, the two helper viruses, and 5 to 7 days later, the EnvA-ΔG-mCherry rabies virus were injected in the lumbar spinal cord in control mice ($n = 5$) to evaluate the presence of mCherry, which would indicate leak expression of TVA and subsequent rabies infection in the absence of Cre. Previous studies have found that dilution of the helper virus is an important factor to achieve efficient trans-synaptic labeling in Cre mice and to avoid background labeling in Cre-negative control mice (Lavin et al., 2020). Here, a 1:20 mix of helper viruses AAV9-CAG-FLEX-oG-WPRE-SV40-pA and TVA-GFP helper virus was used, since larger amounts of the former were found to kill infected cells (data not shown). The injected amount corresponded to approximately 4.45×10^6 viral genomes of the AAV9-CAG-FLEX-oG-WPRE-SV40-pA virus and 2.109×10^8 viral genomes of the TVA-GFP helper virus. The subsequent histological analysis showed that all control animals were injected around L4/L5 and identified two GFP-expressing cells and one GFP/mCherry cell, indicative of a double TVA-GFP virus/EnvA-ΔG-mCherry rabies virus-infected cell at the ipsilateral side in a spinal cord section from one animal. Despite this low number of GFP-expressing neurons, a moderate number of cells with mCherry expression in
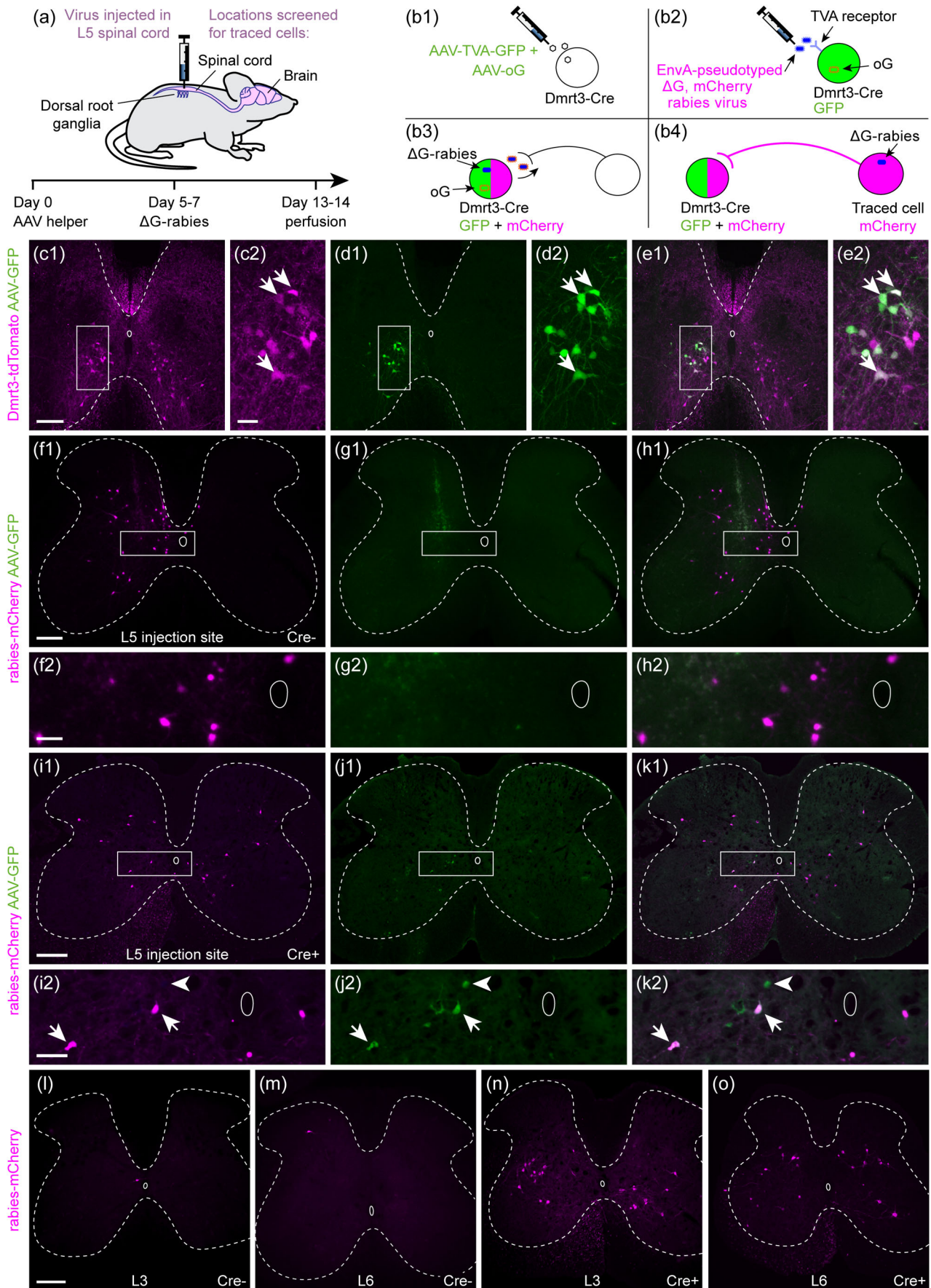
FIGURE 1 Inputs to lumbar Dmrt3 neurons can be retrogradely traced using a recombinant rabies virus strategy. (a) Helper AAV and recombinant rabies viruses were injected unilaterally in the lumbar spinal cord to retrogradely trace their presynaptic inputs. (b) AAV helper viruses containing Cre-dependent TVA-GFP and oG constructs were injected first (b1), followed by EnvA-pseudotyped ΔG, mCherry rabies virus

TABLE 4 Summary of the analysis of GFP and mCherry cells found in the spinal cord and brain of control animals

Mice	Number of spinal cord GFP cells ipsilateral	Number of spinal cord mCherry cells ipsilateral	Number of spinal cord mCherry cells contralateral	Spread of the cells in the spinal cord (mm)	Percentage of cells at 1 mm from injection site (%)	Number of cells in brain
Control 1 Cre-	0	200	6	1.8	95	0
Control 2 Cre-	2	92	2	1.9	79	2 (medulla)
Control 3 Cre-	1	490	9	4.3	78	1 (Cortex), 1 (medulla)
Control 4 Cre-	0	36	3	1.1	92	0
Control 5 C57Bl/6	0	89	2	1.4	87	0

the spinal cord was identified, which was restricted to the site of injection (Figure 1f–h and Table 4). In the five control mice analyzed, an average of 182 mCherry cells at the proximity of the injection sites were identified (with control animal 3 having 499 cells and the remaining four animals had less than 210 cells) (Table 4). In control animal 3, with the highest number of cells, we noticed increased scar tissue around the injection site, suggesting that mechanical injury at the time of virus injection might have promoted unspecific infection. The unspecific infection with the EnvA-ΔG-mCherry rabies virus in control animals was mainly restricted to the ipsilateral side and to approximately two segments (around 2 mm) of the spinal cord with more than 79–95% of the cells being restricted to only one segment (n = 4 animals). However, for control animal number 3 with the higher number of cells, the cells were spread to approximately four segments with more than 78% located in approximately one segment around the injection site (Table 4). An average of 4.8 mCherry-expressing cells and no GFP-expressing cells were found on the contralateral side (n = 5 animals). In comparison, in experimental Dmrt3-Cre+ animals, we found thousands of mCherry-expressing cells along the entire length of the spinal cord (from 1255 to 14,125 cells), with similar numbers on both sides of the spinal cord and less than 40% located within one segment around the injection site (n = 3 animals) (please see the detailed analysis further down). These control experiments demonstrated that the concentration of helper viruses used led to a minor leakage of the TVA, mainly restricted to the injection

site and with almost no mCherry expression on the contralateral side.

In the lumbar dorsal root ganglia (DRG) of the Cre-negative control mice (n = 5 animals), an average number of 4.6 neurons were found, consistently located in ipsilateral lumbar DRG. Notably, 19 out of the 23 cells counted were found in two DRG from control animal 3, having the highest number of mCherry neurons in the spinal cord as described above. In the brain, a total of four cells were found (n = 5 animals), three cells in the medulla, and one cell in the cortex (Table 4). Thus, very few traced neurons were found in control tissue from brain, DRG, and spinal cord segments outside of the injection site, demonstrating the low rate of TVA leakage with our method. We therefore consider that the results obtained from the Dmrt3-Cre-based tracing experiments are reliable and appropriate for identifying neurons making presynaptic connections onto spinal cord Dmrt3 interneurons.

3.2 | Both intra- and intersegmental spinal neurons contact spinal Dmrt3 neurons

To evaluate the presynaptic input to adult spinal Dmrt3 neurons, the two helper viruses and the EnvA-ΔG-mCherry rabies virus were injected in five Dmrt3-Cre+ mice. The expression of GFP (TVA-GFP helper virus-infected cells) was found in the lumbosacral spinal cord,

(b2). The TVA receptor allows entry of EnvA-pseudotyped rabies virus into the cells and oG allows the packaging of rabies genomes for retrograde monosynaptic spread (b3). Dmrt3 estimated starter cells will be marked by GFP (green) and mCherry (pseudocolored magenta), and retrogradely traced cells with only mCherry (magenta) (b4). (c1–e1) with enlargements (c2–e2): The specificity of the helper virus TVA-GFP was confirmed using the Dmrt3-Cre/tdTomato reporter line. After unilateral injection of TVA-GFP, green fluorescence was almost exclusively found in tdTomato (pseudocolored magenta) Dmrt3 neurons. Arrows indicate double positive cells. (f1–h1), with enlargements (f2–h2): In Cre-negative control mice injected with AAV helper and rabies virus, GFP expression was not observed but mCherry-positive cells were found close to the injection site. (i1-k1) with enlargements (i2-k2): In Dmrt3-Cre+ mice injected with AAV helper and rabies virus, double labeled cells were found around the site of viral injection (arrows). Green cells, infected only with AAV helper but not rabies virus (arrowhead), were also found. (l, m) In Cre-negative AAV helper and rabies injected controls, mCherry-expressing cells were scarce at level L3 and L6, outside the injection site. (n, o) In Dmrt3-Cre+ AAV helper and rabies injected animals, many mCherry-labeled traced cells were found at L3 and L6. Injected side is left in all micrographs. (f–h and l–m) are 60 µm thick vibratome sections whereas (c-e, i-k and n–o) are 20 µm cryosections. Scale bars: 200 µm in (c1, f1, i1, l), l also applies to (m, n, o); 50 µm in (c2, f2, i2)

and cells co-expressing GFP and mCherry were found in all injected Dmrt3-Cre mice. More specifically, at level L5 for three animals (animals 3, 4, and 5), at both level L5 and L6 for one animal (animal 1, the only Dmrt3-Cre mouse that received two injections of the modified rabies virus), and more caudally at level S1 for the last one (animal 2) (Figure 1i–k, Figure S1 and Table 1). An estimate of the relative numbers of starter cells between animals was made by assessing GFP/mCherry double labeling. This is likely an overestimate because not all TVA-GFP+ cells will be coinfected with the second helper virus and express the rabies glycoprotein required for rabies spread. Nevertheless, because the rate of co-infection should be similar for all animals, this estimate allows quantitative comparisons across animals. The number of estimated starter cells (GFP/mCherry) varied from 60 to 130 per animal, except for animal 4, which contained less than 10 estimated starter cells. They were found only ipsilateral, except for animal 2 (with injection site at the S1 level), which had around 10% of the estimated starter cells on the contralateral side. We therefore excluded this animal from quantifications and specifically comment only if the tracing pattern from this animal differs from the other animals.

Whereas the number of ipsilateral mCherry-expressing cells was similar in controls and Dmrt3-Cre+ animals close to the injection site, the controls were largely devoid of mCherry expression on the contralateral side and outside the injection site. At L3 and L6, very few mCherry-expressing cells were found in control animals (Figure 1l,m) compared to Dmrt3-Cre+ animals (Figure 1n,o). The number of cells per spinal cord section in Dmrt3-Cre+ animals was highest in the tissue close to the injection site in the lumbar spinal cord, and cells were also found at the thoracic and cervical levels (Figure 2a). The locations of traced cells at different sites along the spinal cord were plotted, where each plot is a summary of the total number of cells on 25 20-μm sections (Figure 2b–e and Figure S2). At the cervical level, most of the traced cells were observed in the ventromedial part of the gray matter with a slightly higher number of cells in the contralateral side for three animals (Figure 2b and Figure S2). At the thoracic level, a higher number of cells was found in the ventral part, with a moderately higher number in the contralateral side compared to ipsilateral as well for three animals. Fewer cells were found in the dorsal part where they were mainly localized in layer V–VI (Figure 2c and Figure S2). At the lumbar level, the distribution between the ipsilateral and contralateral side appeared more differentiated (Figure 2d and Figure S2). In the ipsilateral side, traced cells were predominantly found in lamina IV to VI of the dorsal horn. In the contralateral side, cells were more aggregated in the mediodorsal part of the ventral horn where commissural interneurons are known to reside (Eide et al., 1999), and accordingly, fibers were seen decussating in the ventral commissure (Figure 2f2,f3, arrowheads). Regarding the localization pattern of the traced cells in the sacral part, it differed between the animals injected at L5 and the ones injected at L6/S1 (Figure 2e and Figure S2). For the former (animals 3 and 5), there was a higher number of traced cells in the ventro-lateral region. Animal 1 also displayed traced cells in the ventral region, but many of them were also concentrated in the deep dorsal horn lamina IV–V and above the central

canal at the level of the sacral dorsal commissure (SDcom) (Watson et al., 2009).

Consistently for all the segments of the spinal cord, traced cells were largely excluded from the superficial dorsal horn, lamina I-III, where the ventral border of lamina II was identified by expression of protein kinase C, gamma (PKCγ) (Figure 2b–e). In addition, almost no cells were found in the deep ventral horn where the alpha motor neurons are located (Figure 2b–e and Figure S2). To begin to identify spinal cord subpopulations that connect to Dmrt3-Cre+ neurons, immunostainings were performed using a panel of available and working markers for different population of neurons in the adult spinal cord (Figure 2f–k). The analysis disclosed that six traced cells expressed choline O-acetyltransferase (ChAT) (2 ipsi/4 contra in 40 sections counted, $n = 2$ animals) among which three were located in close proximity of the central canal, suggesting that they belong to the $V0_C$ population (Zagoraiou et al., 2009) (Figure 2f,i). However, as expected, no traced cells were found in the deep ventral horn overlapping with ChAT, showing that motor neurons do not project onto Dmrt3 neurons. The analysis further demonstrated that 12 traced cells co-expressed Calbindin1 (CALB1) (nine ipsi/3 contra in 39 sections, $n = 2$ animals), where three were located in the ipsilateral deep ventral horn, which indicate that they might be Renshaw cells (Carr et al., 1998) (Figure 2g,j). The analysis also identified 30 traced cells co-expressing Chx10 (Ceh-10 homeodomain-containing homolog also known as VSX2; 30 in 63 sections counted, $n = 2$ animals) (Ericson et al., 1997), a marker for the V2a population; 83% of them (25/30) were situated in the ipsilateral side (Figure 2h,k).

3.3 | Proprioceptive neurons in DRG make monosynaptic connections with spinal Dmrt3 neurons

In the Dmrt3-Cre+ animals, many traced cells were found in the lumbar DRG, primarily on the ipsilateral side (Figure 3a). In whole mount DRG preparation, 184 neurons were identified in the ipsilateral DRG, and somewhat surprisingly, 56 traced neurons were also found in the contralateral DRG ($n = 4$ animals). In total, 240 neurons were found in the four Dmrt3-Cre+ animals, which is substantial compared to the 23 neurons observed in the four control animals. Immunohistochemistry (Figure 3b–j) displayed co-labeling with NF200 (also known as Nefh, neurofilament, heavy polypeptide) in about 97% of the traced neurons (31/32 cells, $n = 3$ animals), indicating that most of them are large myelinated mechanoreceptive neurons (Figure 3c). Furthermore, 68% expressed Calbindin (23/34 cells, $n = 2$ animals), whereas 90% of the traced cells expressed Parvalbumin (65/73 cells, $n = 2$ animals), indicating that the traced cells belong to the Aα proprioceptive subtype (Usoskin et al., 2015; Zheng et al., 2019) (Figure 3d,e). Recently, a mouse DRG single cell transcriptomic study identified markers for different subtypes of proprioceptive neurons (Wu et al., 2021). The study identified Calretinin and Brn3c (brain-specific homeobox 3c also known as Pou4f3) as markers for subtype Ia3 and Ib, respectively, and Calbindin as a marker for Ia2 and Ia3 subtypes. We found that 16% of
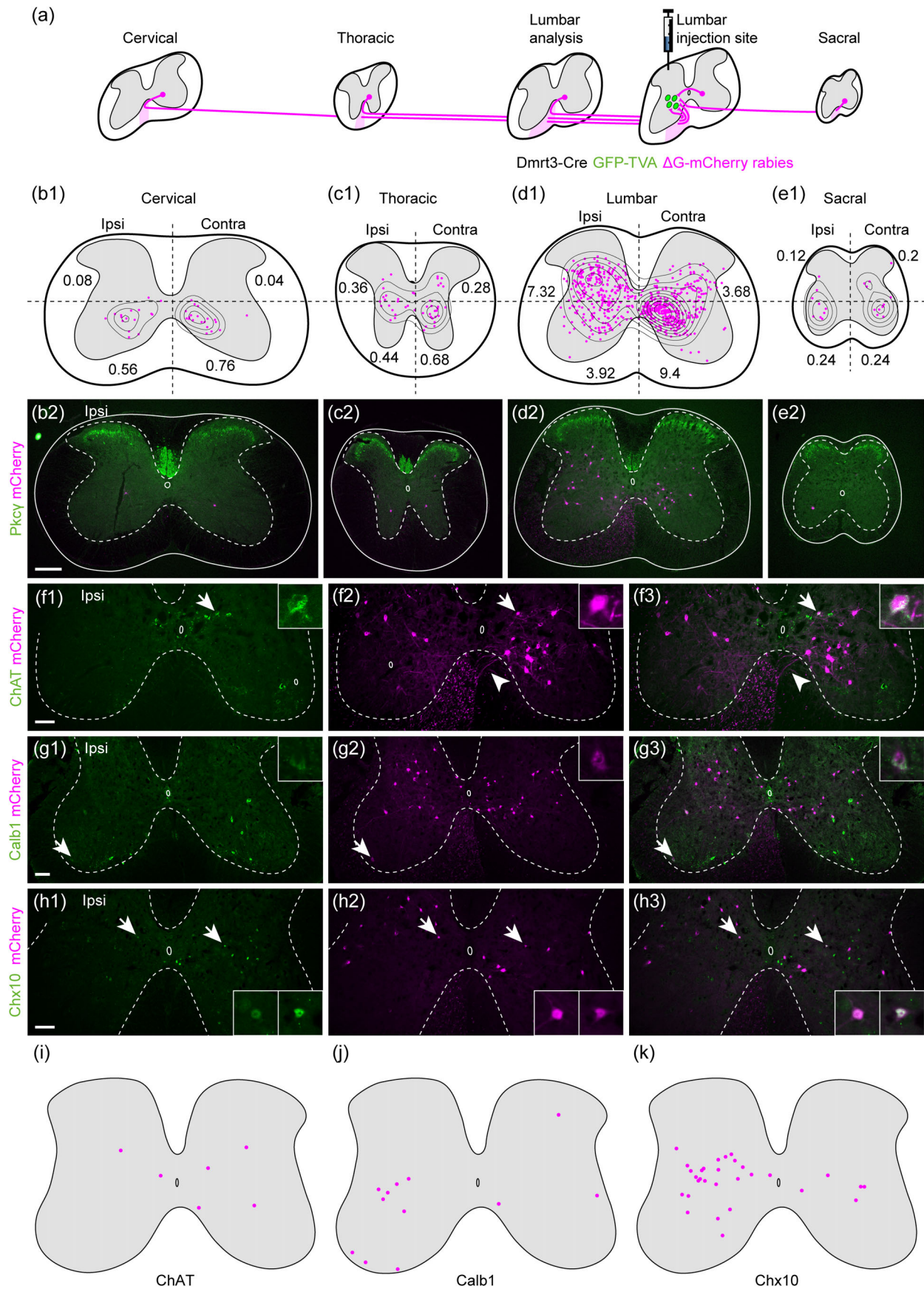
FIGURE 2 Presynaptic cells to spinal Dmrt3 neurons are found at cervical, thoracic, lumbar, and sacral levels. (a) Schematic illustrating that traced cells expressing mCherry (magenta) are found along the entire spinal cord axis, with the highest concentration in the lumbar segments close to the injection site. (b1–e1) Location of traced neurons at different axial levels with density curves. Each drawing shows the combined plots of 25

the counted traced cells expressed Calretinin (5/31 cells, $n = 2$ animals) and 45% expressed Brn3c (5/11 cells, $n = 2$ animals) (Figure 3f,g). This indicates that spinal Dmrt3 neurons receive input from Ia3 and Ib subtype primary afferents, and most likely Ia2 based on the high number of Calbindin-positive cells in relation to the markedly lower number of Calretinin-positive cells.

In addition, none of the analyzed traced cells were positive for CGRP (calcitonin gene-related protein, 0/21 cells, $n = 1$ animal), IB4 (Isolectin B4, 0/57 cells $n = 3$ animals) or TH (Tyrosine hydroxylase, 0/25 cells, $n = 2$ animals) (Figure 3h–j), which indicate that spinal Dmrt3 neurons do not receive input from primary sensory neurons involved in nociception (Usoskin et al., 2015; Zheng et al., 2019). Rabies virus does not infect all cell types, can be cytotoxic, and in DRG, TH- and IB4-expressing neurons are difficult to infect (Albisetti et al., 2017). However, IB4 neurons have been successfully traced (Sun et al., 2017), indicating that our result regarding the absence of traced nociceptive neurons is valid. Together, these data demonstrate that spinal Dmrt3 neurons receive inputs primarily from proprioceptive primary sensory neurons, including neurons of the Ia3 and Ib subtypes.

Somewhat surprising to us, we found a substantial part of the connected cells in contralateral DRG (23%). Functional links between the two sides of the spinal cord have been described previously, for example, unilateral pain stimulation induces bilateral changes in dorsal horn cells (Fitzgerald, 1982). Moreover, tracing studies have identified nociceptive primary afferents that terminate within the dorsomedial and dorsolateral regions of the contralateral spinal cord (Comer et al., 2015). However, our characterization of traced DRG cells suggests that contralateral inputs to Dmrt3 neurons are also predominantly proprioceptive. Previous descriptions of contralateral proprioceptive primary afferents are scarce in the literature; however, neurons targeted by proprioceptive neurons have been found in the contralateral ventral horn (Pimpinella & Zampieri, 2021). Another possibility is that Dmrt3 interneurons, in addition to midline decussating axons, also extend commissural dendrites, as it has been found in medial motor column motor neurons (Goetz et al., 2015). Our analysis of MAP2 expression, a dendrite marker, however, suggest that Dmrt3 interneurons do not send commissural dendrites but send an extensive number of axons in the contralateral ventral horn (Figure S3). Thus, one explanation could be that the primary afferents make axo-axonic contact with contralateral axons of the Dmrt3 neurons. Although limited, there is evidence that the rabies virus can be transmitted by axo-axonic synapse (Zampieri et al., 2014). Moreover, at least in zebrafish, a subtype of the Dmrt3 neurons was shown to make axo-axonic contacts with spinal motor neurons (Kishore et al., 2020).

3.4 | Traced neurons were found in brainstem and cortex regions involved in motor regulation

Dmrt3 neurons receive presynaptic terminals containing markers for aminergic transporters, suggesting that they receive modulatory inputs from the monoaminergic systems (Perry et al., 2019). We next investigated whether neurons in higher brain centers project to the Dmrt3 neurons.

We found 154 traced cells in the red nuclei ($n = 3$ animals) (Figure 4a,b). In animal three, there was a higher number of traced cells in the contralateral nucleus (2 ipsilateral, 42 contralateral), whereas in the other two animals (animals 1 and 5), the number of cells were more similar in the ipsi- and contralateral nucleus (17 ipsilateral and 39 contralateral; 25 ipsilateral and 29 contralateral). Traced cells were found in the ventrolateral region of the red nucleus, an area including the magnocellular part that projects to spinal lumbar levels (Liang et al., 2012). Fibers decussating between the red nuclei, at the location of the ventral tegmental decussation of the rubrospinal tract and continuing ventrally between the red nucleus and the ventral tegmental area were also identified (Figure 4b). At cervical levels of the spinal cord, mCherry-positive projections were found in the dorsal part of the lateral funiculus and lateral to the spinal nucleus, in the location of the rubrospinal tract (Liang et al., 2012) (Figure 4c). The rubrospinal tract is known to be contralateral in humans, but some projections have been found on the ipsilateral side at spinal levels in rodents potentially explaining the bilateral innervation found here (Antal et al., 1992; Liang et al., 2012).

Furthermore, in three animals, two to three traced neurons per animal were found in the ipsilateral lateral periaqueductal gray region (PAG) (Figure 4d,e). The dorsal and lateral periaqueductal gray have been associated with altered motor behavior in the presence of a potential threat or via optogenetic activation (Deng et al., 2016; Mendes-Gomes et al., 2020). It is thus possible that neurons in the lateral periaqueductal gray that contact spinal Dmrt3 neurons may be involved in regulating supraspinal-induced motor behavior.

The remaining brainstem analysis was performed on the brains from animal 3 and 5 since the brainstem of animal 1 was sectioned differently from the reference brain atlas, and although many cells were mCherry positive, the regions in which they were located were obscure. Traced cells were found bilaterally in the pontine reticular nuclei, both in the rostral (oral) and caudal parts (PnO: 61 cells ipsilateral and 41 cells contralateral and PnC: 10 cells ipsilateral and 4 cells contralateral, $n = 2$ animals) (Figure 4d–f). The mouse oral pontine reticular nuclei project to the entire spinal cord with fibers in the ipsilateral ventral funiculus terminating in laminae VII–X and some

20-µm sections. The number in each quadrant represents the average number of traced cells per section in that quadrant. (b2–e2) show representative examples of sections from each level. Tissue was counterstained with anti-PKCγ (green). (f–h) Subtype-specific markers revealed a small number of traced neurons expressing ChAT, Calb1 (Calbindin), and Chx10. Arrows indicate double-positive cells shown in magnification. Arrowheads in f2 and f3 show decussating axons. (i-k) summarize the locations of traced cells positive for each marker. All scale bars 100 µm, for magnifications 20 µm. Scale bar in (b2) applies to (b2-e2)
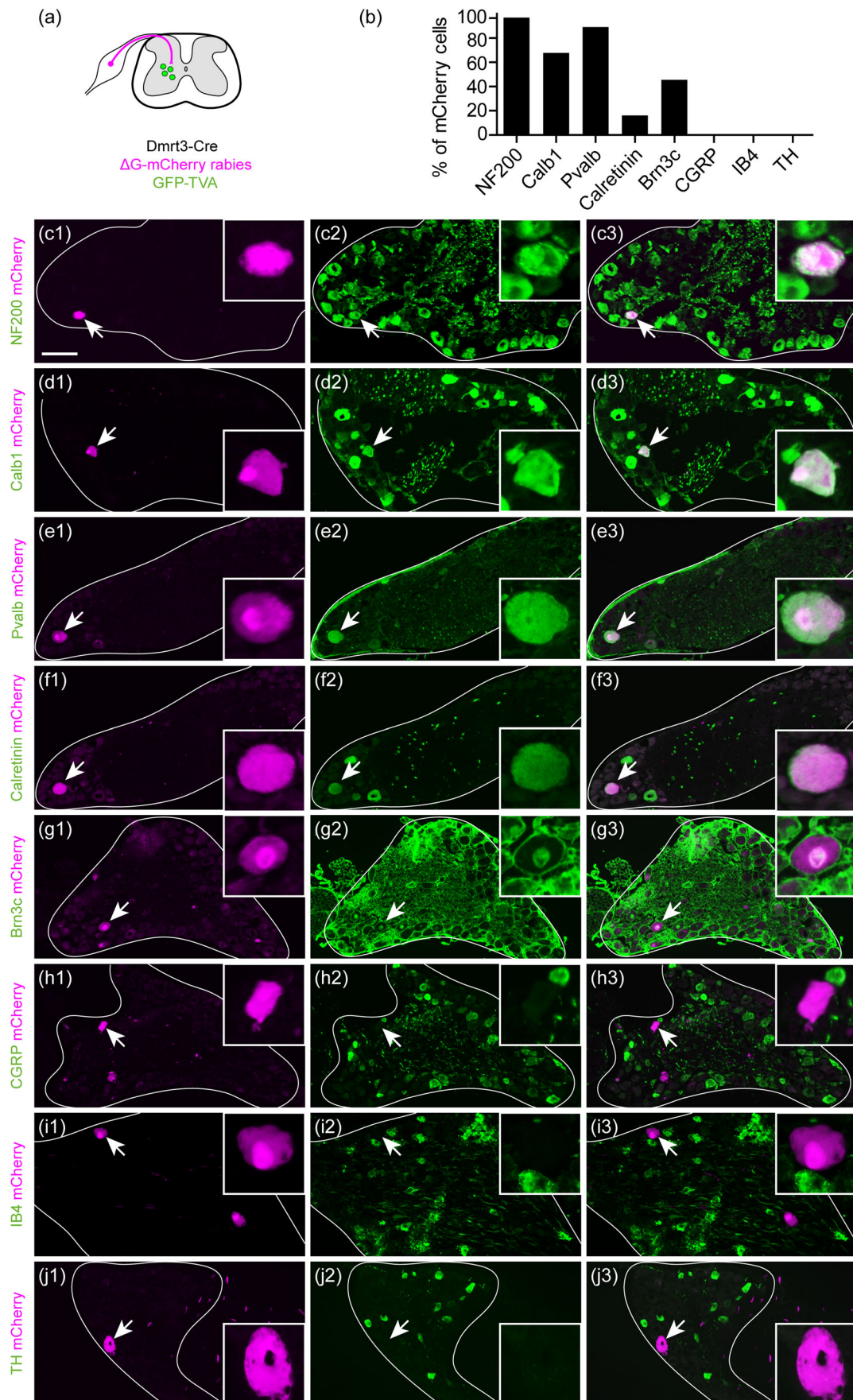
FIGURE 3 Spinal Dmrt3 interneurons are contacted by proprioceptive afferents. (a) Traced primary afferent neurons were found in ipsi- and contralateral DRG with an ipsilateral predominance. (b–j) Among ipsilateral traced cells, a majority expressed markers for myelinated neurons (NF200 [Nefh] and calbindin [Calb1]) and proprioceptive marker parvalbumin (Pvalb). Subsets of traced neurons expressed proprioceptive

collaterals in the contralateral lamina VII (Liang et al., 2015). The caudal part of the pontine nuclei (PnC) has a similar projection pattern but with higher density of fibers in laminae VII and VIII in the lumbar and sacral segments compared to the rostral part (Liang et al., 2015). Rubrospinal projections were also seen in the pons, lateral to the pontine reticular nucleus (Figure 4e2).

In the medulla, traced cells were found on both sides, near the fourth ventricle, which corresponds to the location of the lateral (LVe) and spinal vestibular nuclei (SpVe) (LVe: 36 cells ipsilateral and 23 cells contralateral, SpVe: 10 cells ipsilateral and 10 cells contralateral, $n = 2$ animals) (Figure 4g–k, rostral to caudal).

The medial parts were devoid of labelled cells, in line with the notion that the cells of the medial vestibular nucleus do not project to the lumbar level of the spinal cord (Watson & Harrison, 2012). The lateral and spinal vestibular nuclei relay information from the otoliths for righting of body posture in response to body imbalance, while the medial vestibular nuclei relay information from semicircular canals for autonomous control of head movements. A limited number of traced cells were also found in the superior vestibular nuclei, which seem to be involved in eye movement control (SuVe: 13 cells ipsilateral and 9 cells contralateral) (Watson et al., 2011). Traced axons were observed in the ventromedial white matter of the cervical spinal cord where the vestibulospinal tract is located (Figure 4c4).

The caudal medulla also contained traced cells on both sides, mainly in the gigantocellular reticular nuclei (Gi: 56 cells ipsilateral and 26 cells contralateral, GiA [alpha]: 10 cells ipsilateral and 10 cells contralateral, GiV [ventral]: 2 cells ipsilateral and 4 cells contralateral, LPGi [lateral paragigantocellular nuclei]: 5 cells ipsilateral and 8 cells contralateral; $n = 2$ animals) (Figure 4g, i–k). The gigantocellular nuclei project to the spinal cord, join the reticulospinal tract (ReST) in the ventrolateral funiculus (Figure 4c5) and innervate ventral spinal laminae. In the caudal part of the medulla, axons from traced cells extended dorsomedial, likely to join the medial longitudinal fascicle in their course towards the spinal cord. The ReST relays motor-relevant neuronal commands from the reticular formation to central pattern generator units in the spinal cord (Liang et al., 2016). A small number of traced cells were also found in the intermediate/parvocellular reticular formation of the medulla (4 cells ipsilateral and 6 cells contralateral, $n = 2$ animals) as well as the medullary reticular formation ventral part (4 cells ipsilateral and 3 cells contralateral, $n = 2$ animals, data not shown).

Further, traced cells were found in the ventral and caudal raphe nuclei (Figure 4k) that modulate motor circuit activity by release of serotonin (10 cells; $n = 2$ animals). Fibers from these nuclei descend to the spinal cord in the ventrolateral white matter and terminate in the intermediolateral cell column and on motor neurons in the ventral horn (Bowker et al., 1982; Tracey, 2004).

In animal 2, excluded from quantifications due to bilateral presence of estimated starter cells, we found traced cells in the same brain regions as the other animals, and in addition, we identified nine cells in the Barrington nucleus involved in micturition. The other animals did not contain any cells in this nucleus, thus, a possible explanation is the more caudal site of the injection in the S1 segment for animal 2, where projections from the Barrington nuclei are known to terminate (Kawatani et al., 2021; Verstegen et al., 2017). For all animals, we did not observe traced cells in nuclei of other descending tracts in the hypothalamus, prethalamus, midbrain, pons, and medulla.

Although scarce, traced cells were repeatedly found in the ipsi- and predominantly in the contralateral motor and somatosensory cortex (5 cells ipsilateral and 12 cells contralateral, $n = 3$ animals) in an area that has previously been demonstrated to contribute corticospinal projections to lumbar levels (Wang et al., 2018) (Figure 5a,b). Labeled cells had a pyramidal shape (Figure 5c–f) and were located in cortical layer V (Bregma −0.34 mm to −1.06 mm). The role of the corticospinal tract for locomotion and motor control is well established, and in humans, direct projections to lower motor neurons are present. However, the main area of termination in rat is in the medial part of the deep dorsal horn and the intermediate gray matter, in laminae III–VII (Brown, 1971), reflecting its indirect control of limb movements.

4 | DISCUSSION

To reach in-depth understanding of mature neuronal circuit function, a thorough analysis of the participating components is required. Here, we focused on adult spinal cord Dmrt3 interneurons that are involved in the control of locomotion, and searched for the origin of their presynaptic inputs using EnvA-pseudotyped rabies tracing.

4.1 | Methodological considerations

Our study showed that the EnvA-ΔG-mCherry rabies virus monosynaptic retrograde tracing is a powerful technique to identify the presynaptic neurons, making contacts to the spinal Dmrt3 interneurons. However, some methodological limitations have to be taken in account while interpreting the data.

Firstly, we performed tracing on five Dmrt3-Cre+ animals, but due to the limitations and challenges of viral-based tracing, we removed two of them from the quantitative analysis. Animal 2 was excluded from analysis because we found cells expressing TVA-GFP+ in the contralateral side, and animal 4 was excluded from brain and DRG analysis because of a very low number of traced cells in this animal. Moreover, for animal 1, spinal cord sections were mounted without IHC analysis, and DRG were not kept after having performed wholemount imaging. Thus, IHC on the spinal cord and DRG was performed on sections from two animals, and the location of mCherry neurons in the cerebrum and midbrain was analyzed in three animals (except for the pons and

---

subtype markers Calretinin and Brn3c, but no co-labeling with markers for unmyelinated thermo/nociceptive neurons CGRP (Calca), IB4 nor TH was found. Arrows indicate traced cells shown in enlargements. (e and f) are adjacent sections of the same cell. For (g), note that Brn3c is a nuclear marker and the staining of membranes is unspecific. Scale bar in (c) equals 100 μm and applies for (c-j), 25 μm for all enlargements
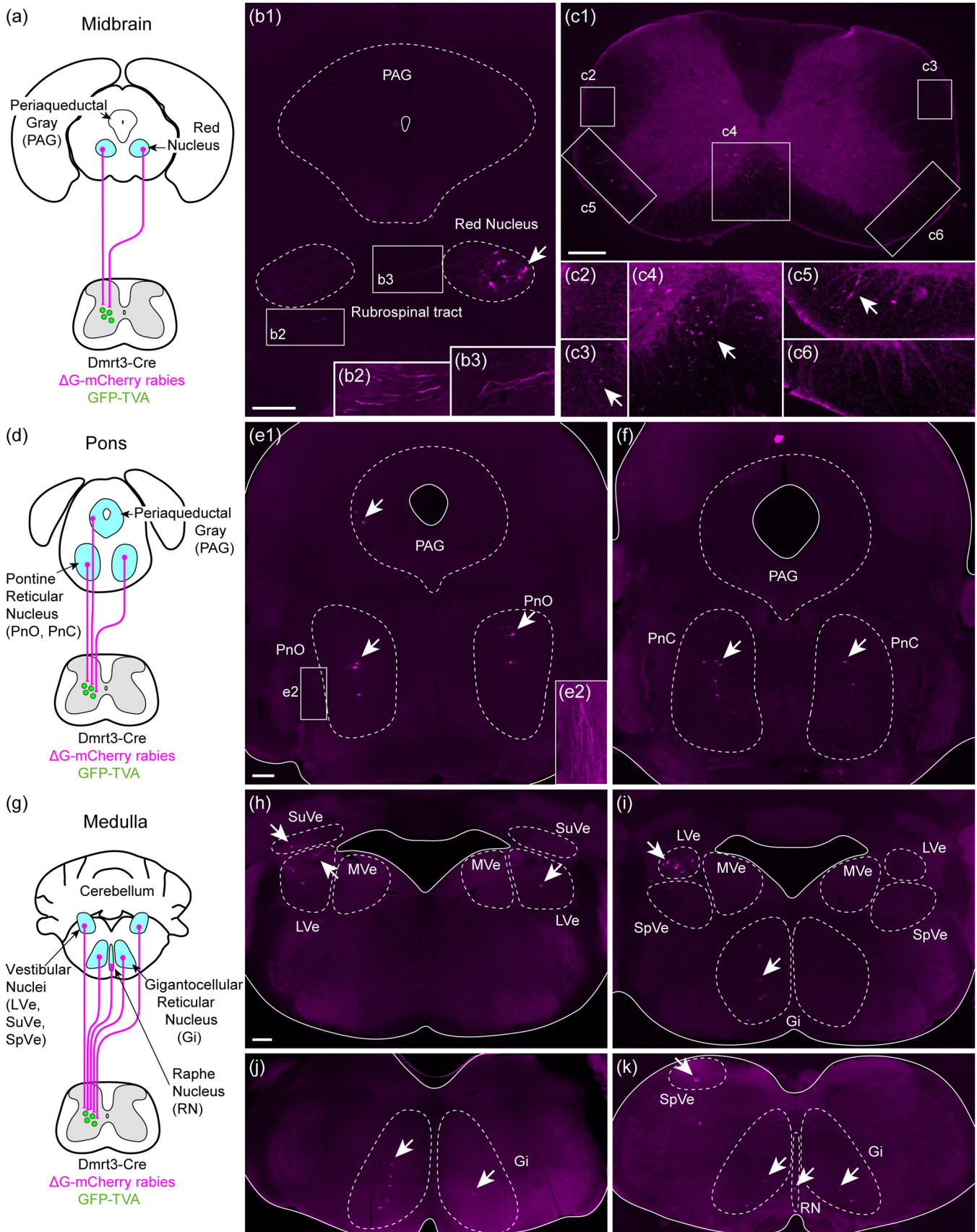
FIGURE 4 Spinal Dmrt3 neurons receive input from brainstem areas involved in motor control. (a, b) In the midbrain, traced cells were found in the red nucleus, mainly in the lateral part and with a contralateral predominance. Magnifications (b2, b3) with increased brightness and contrast show projections of the rubrospinal tract around the red nuclei. (c) Traced axons were found in the spinal cord at the cervical level mainly in the

VIEILLARD ET AL.

JCN
RESEARCH IN
SYSTEMS NEUROSCIENCE
THE JOURNAL OF COMPARATIVE NEUROLOGY

WILEY 19

medulla which was done in two animals). The small number of animals might affect the reliability of our study; however, even if animal 2 was excluded from the quantifications because of the presence of contralateral GFP cells, we found mCherry cells in the same brain and brainstem region as well as similar primary sensory neuron subtypes when performing IHC (data not shown).

Secondly, rabies virus is known to modify the transcriptional program of infected cells in the mouse brain (Huang & Sabatini, 2020; Prosniak et al., 2001). A recent study, which performed single cell nuclei RNA sequencing on cortical cells infected with an EnvA-ΔG-rabies virus, found that the expression of some neuronal markers was affected. For example, the expression of somatostatin, parvalbumin, and vasoactive intestinal peptide (VIP) was down-regulated in neurons infected with the rabies virus. When performing a fluorescent in situ hybridization, they showed that the detection of somatostatin mRNA was decreased in cells infected with EnvA-ΔG-rabies virus (Patiño et al., 2022). This data suggest that the results from IHC on cells infected with rabies virus should be taken with caution since some of the EnvA-ΔG-mCherry rabies virus infected cells in this study may have been devoid of an investigated marker due to rabies virus-induced gene down-regulation.

Finally, we unexpectedly found traced neurons in the ipsilateral red nucleus (2 brains out of 3) and the contralateral lateral vestibular nucleus (1 brain out of 2) as well as traced cells in the contralateral DRG (4 animals). We did not observe Dmrt3 neuron dendrites in the contralateral side (Figure S3). However, Dmrt3 neurons send axonal projection to the contralateral side; thus, one possible explanation could be axo-axonic synapses. For these four animals, we did not find any expression of TVA-GFP in the contralateral side near the injection side. However, the presence of low-expressing GFP cells in the contralateral side cannot be ruled out, which could be another potential explanation.

4.2 | Brainstem areas projecting to Dmrt3 interneurons are related to motor function

Previous retrograde tracing experiments, albeit from cervical segments, have identified 27 brain centers projecting to the spinal cord (Nudo & Masterton, 1988) and 25 subregions were found from lumbar tracing experiments (Wang et al., 2021). In our whole-brain analysis of Dmrt3-Cre+ animals, we found traced cells in the motor/somatosensory cortical areas, in the red nuclei, PAG, pontine reticular nuclei, vestibulospinal nuclei, gigantocellular nuclei, and raphe nuclei (Figure 5g). These brain areas are associated to motor function. For example, the majority of the rubrospinal fibers are excitatory and terminate in contralateral laminae V, VI, and the dorsal part of lamina VII at all spinal cord levels, which is consistent with the position of Dmrt3 interneurons (Liang et al., 2012). Studies in various species have found that the red nucleus is important for sensorimotor integration and locomotion via connections with interneurons and motor neurons in the spinal cord. The red nucleus is present in animals with limbs, wings or fins, and connections between the red nucleus and the spinal cord appeared during the transition from aquatics to amphibians. Thus, the development of structured limbs requiring more intricate limb control may involve Dmrt3 interneurons connected to the red nucleus (Basile et al., 2021; Holstege et al., 1988; Küchler et al., 2002; Nyberg-Hansen, 1966; Nyberg-Hansen & Brodal, 1964; ten Donkelaar & de Boer-van Huizen, 1982; Warner & Watson, 1972; Wild et al., 1979).

Moreover, pontine pathways are thought to be involved in muscle atonia during REM sleep, a hypothesis that needs confirmation. The caudal part of the PnC, where traced cells were found, project to lumbar and sacral segments (Liang et al., 2015), indicating an involvement in hindlimb motor control.

4.3 | Spinal Dmrt3 neurons are part of circuits involved in sensorimotor integration

Abundant presynaptic neurons were found at different levels of the spinal cord, although the number of connected neurons gradually decreased with increased distance from the estimated starter cells. At the cervical and thoracic level, the traced neurons were mainly localized in the ventral horns. These direct inputs to Dmrt3 neurons from ventrally located neurons at cervical levels suggest a possible connectivity with neurons involved in the forelimb CPG. At the lumbar level, ipsilaterally connected neurons were predominant in the deep dorsal horn, whereas contralateral neurons were found more medioventral at the expected location for commissural interneurons (Eide et al., 1999). The majority of connected cells in the spinal cord remain genetically unidentified; however, a portion of the cells could be classified using immunohistochemistry with markers present in adult animals in spinal cord populations of interest.

First, the analysis identified traced cholinergic cells near the central canal; such presumptive $V0_C$ interneurons project to and activate

---

ipsilateral ventromedial white matter (location of vestibulospinal and reticulospinal tracts, (c4, c5)) and on the contralateral side at the location of the rubrospinal tract (c3) (indicated with arrows). Almost no projection was observed on the ipsilateral side at the location of the rubrospinal tract (c2). (d–f) In the pons, traced cells (indicated with arrows) were found bilaterally in the pontine reticular nucleus oral (PnO) and caudal (PnC) parts. Projections of the rubrospinal tract were seen laterally (magnification e2 with increased brightness and contrast). A small number of cells were found in the ipsilateral lateral PAG. (g–k) In the medulla, traced cells (indicated with arrows) were found bilaterally in the lateral, superior, and spinal vestibular nuclei (LVe, SuVe, and SpVe, respectively) with an ipsilateral predominance, but not in the medial vestibular nucleus (MVe). Labeled cells were found bilaterally in the gigantocellular reticular nucleus (Gi) and in the raphe nuclei (RN). (h–k) represent a rostral to caudal progression of the medulla. Dashed lines demarcate approximate borders of relevant anatomical structures, unbroken lines represent the edge of the tissue. Ipsilateral is left in all images. All scale bars 250 μm, for magnifications (b2, b3) 167 μm, for magnifications (c2–c6) and (e2) 125 μm. Scale bar in (e1) also applies to (f). Scale bar in (h) applies to (h-k)
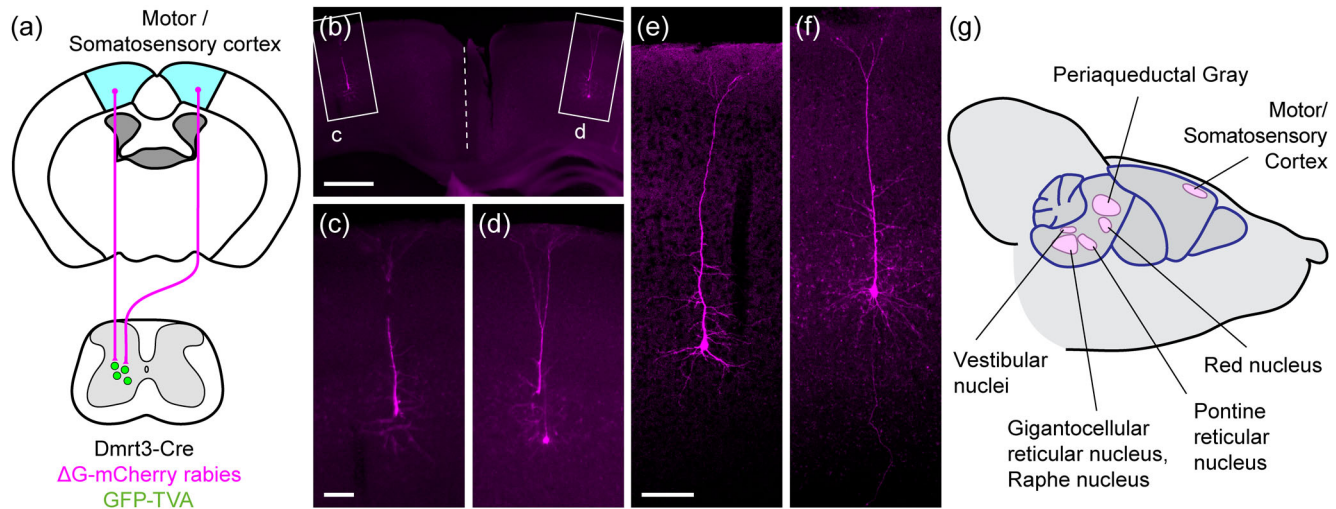
FIGURE 5 Spinal Dmrt3 neurons receive input from neurons found in primary motor/somatosensory cortex. (a) Cells from the medial part of the cortex, approximately the area of primary motorcortex and hindlimb area of primary somatosensory cortex, are retrogradely traced from lumbar Dmrt3 neurons. (b) With enlargements (c,d), traced cells are found bilaterally and have a pyramidal shape, (e-f) are high magnification confocal images to show further examples of the morphology. Scale bar 500 μm in (b), 100 μm in (c, e) also applies to (d, f). (g) Summary of the main locations of traced cells in the brain.

motor neurons via the so-called C-boutons (Zagoraiou et al., 2009). V0$_C$ cells are thus candidates for connecting to Dmrt3 interneurons, which in turn connect to motor neurons (Andersson et al., 2012). A dispatch of inhibitory signals released from Dmrt3 interneurons to motor neurons could thus stem from V0$_C$ interneurons. If so, V0$_C$ cells would, similar to spinal cord reflex pathways, be endowed with the capability to send activating signals to motor neurons in parallel with reciprocal inhibition via Dmrt3 neurons, a hypothesis that remains to be tested. Our analysis also identified three calbindin-positive cells at the spinal gray ventral rim, defined as Renshaw cells (Carr et al., 1998; Geiman et al., 2000), and the low number found indicate that connections are scarce and probably made to a subset of Dmrt3 interneurons. Even so, this type of connection has been suggested in the context of indirect disinhibitory action onto motor neurons from Ia interneurons, relayed by Renshaw cells (Hultborn et al., 1971).

Further, the analysis revealed traced Chx10-positive V2a excitatory interneurons, mainly in the ipsilateral side of the spinal cord. These interneurons have been demonstrated to be essential for skilled reaching (Azim et al., 2014) and to coordinate left–right limb locomotion (Crone et al., 2008). Furthermore, they contact commissural interneurons in the ventromedial region of the lumbar spinal cord, among which the V0 population reside (Lundfald et al., 2007), and our results indicate that Dmrt3 neurons could also be part of this commissural interneuron population. Moreover, our data demonstrated that Dmrt3 interneurons are contralaterally targeted by a smaller part of the Chx10 population. In some support, midline crossing of Chx10 cell projections was previously observed in the mouse hindbrain (Cepeda-Nieto et al., 2005).

In summary, our data demonstrated that lumbar Dmrt3 interneurons receive inputs from spinal neurons engaged in sensorimotor coordination.

4.4 | Spinal Dmrt3 neurons receive sensory input from both muscle spindles and Golgi tendon organs

We consistently found monosynaptically connected cells in lumbar DRG, and the vast majority of them were classified as large myelinated mechanoreceptive neurons of the Aα proprioceptive subtype. By the use of recently reported markers for subclassification of the proprioceptive neurons (Wu et al., 2021), the analysis further showed that the traced neurons included the Ia2 and the Ia3 subtypes, belonging to group Ia afferents and group Ib afferents. Primary afferents of group Ia contribute to the stretch reflex, through the transmission of signals directly to a homonymous muscle, and a reciprocal muscle connection via inhibitory Ia interneurons to an antagonistic muscle (Eccles et al., 1956). Monosynaptic input from group I afferents preferentially reach commissural interneurons in lamina VII (Jankowska et al., 2009), which is where Dmrt3 interneurons reside in mice. Considering that Dmrt3 interneurons can be commissural and connect to motor neurons both ipsi- and contralateral (Andersson et al., 2012), it is conceivable that this inhibition can be forwarded by Dmrt3 interneurons.

How does proprioceptive input and locomotion relate to each other? It has been shown that the transition of locomotor stance to swing phases involves shifting muscle spindle activation to Golgi tendon organ activation and thus, that coordinated activity from proprioceptors plays a part in initiation and duration of locomotion (Koch, 2019). Group Ia primary afferents are rapidly adapting and report stretch velocity from nuclear bag fibers (Mihailoff & Haines, 2017), while the more thinly myelinated group II primary afferents are nonadapting, mainly transmit signals from nuclear chain fibers reporting muscle length change, and remain active after the muscle ceased moving. Therefore, interneurons that connect to group Ia and group II afferents are presumably separate populations. Dmrt3 neurons can be subclassi-

fied based on their expression of other markers (Andersson et al., 2012; Iglesias González et al., 2021; Schnerwitzki et al., 2018); thus, it will be important to examine how the different types of inputs can be functionally linked to Dmrt3 interneuron subpopulations. Furthermore, it is known that descending tracts connect to Ia interneurons (Hultborn et al., 1976), as well as to lamina VIII commissural interneurons (Bannatyne et al., 2003). In contrast to group Ia afferents, Ib afferents do not monosynaptically connect to motor neurons; instead, they connect to Ib interneurons for protective inhibition of muscle activity in the Golgi tendon reflex circuit. Based on this, we suggest that Dmrt3 neurons can belong to functional subclasses with regard to peripheral input type (Ia and Ib) and descending input type (serotonergic and glutamatergic).

Dmrt3 neurons in the dI6 mouse spinal cord population have previously been divided into functional subtypes (Griener et al., 2017; Perry et al., 2019). A recent single cell sequencing study divided the spinal Dmrt3 neurons from mice into six clusters (M1–6) based on their transcriptomic profile (Iglesias González et al., 2021). Most clusters, except M1, express the 5HT–7 receptor, providing some of the molecular set up required to receive descending serotonergic input from the Raphe nuclei, and it has been reported that interneurons in laminae VII and VIII are likely sites for serotonergic modulation of the centrally activated locomotor network (Noga et al., 2009). The expression of *Neurotrophin-3* (*Ntf3*) was found in the M3 cluster, and to a lower extent, in the M1 cluster. This growth factor molecule binds to TrkC, which is expressed in primary afferents, to transmit a target-derived survival signal specifically between proprioceptive afferents and motor neurons (Ernfors et al., 1994; Klein et al., 1994). Notably, the absence of NTF3 or TRKC resulted in the loss of DRG afferents in both the medial and lateral spinal cord. One possibility is therefore that the M1/M3 clusters of the Dmrt3 interneurons constitute inhibitory interneurons connected to proprioceptive primary afferents.

5 | CONCLUSIONS

In this tracing study, we have investigated the spinal Dmrt3 interneurons and our main conclusions are: (1) the peripheral connectivity of the spinal Dmrt3 population predominantly consist of inputs from proprioceptive primary afferents, positioning Dmrt3 neurons in a sensorimotor integrative role, (2) supraspinal areas involved in autonomous motor control (vestibular, rubrospinal, pontine, and raphe) project to spinal Dmrt3 neurons, (3) lumbar Dmrt3 interneurons receive information from spinal interneurons at all axial levels of the spinal cord.

We show that the functional role of spinal Dmrt3 neurons appears to be more closely linked to sensory processing than previously appreciated. In particular, the connectivity of the Dmrt3 inhibitory interneurons to proprioceptive Ia and Ib primary afferents defines at least part of them to be spinal Ia and Ib interneurons. At limb spinal levels, Ia inhibitory neurons provide reciprocal innervation to flexor and extensor motor pools, and their origin have been suggested to reside within the V1 and V2b cardinal classes of interneurons (Zhang et al., 2014). Our analysis suggests that also Dmrt3 inhibitory interneurons of the dI6 cardinal class contribute to the further transmission of

proprioceptive signaling. It is also clear, however, that the Dmrt3 population is not homogenous; thus, refined techniques to provide a new level of detail regarding the composition of the Dmrt3 population (Iglesias González et al., 2021) will be required to tease out the properties of each of these subpopulations of spinal Dmrt3 interneurons.

CONFLICT OF INTEREST

The authors declare no competing financial interests.

DATA AVAILABILITY STATEMENT

The data that support the findings of this study are available from the corresponding authors upon reasonable request.

ORCID

Jennifer Vieillard https://orcid.org/0000-0003-4319-5154
Marina C. M. Franck https://orcid.org/0000-0002-2174-6392
Sunniva Hartung https://orcid.org/0000-0002-9444-5363
Jon E. T. Jakobsson https://orcid.org/0000-0003-3845-5417
Mikaela M. Ceder https://orcid.org/0000-0002-9681-5129
Robert E. Welsh https://orcid.org/0000-0002-0500-2115
Malin C. Lagerström https://orcid.org/0000-0002-9086-2805
Klas Kullander https://orcid.org/0000-0001-6418-5460

PEER REVIEW

The peer review history for this article is available at https://publons.com/publon/10.1002/cne.25405.

REFERENCES

Akay, T., & Murray, A. J. (2021). Relative contribution of proprioceptive and vestibular sensory systems to locomotion: Opportunities for discovery in the age of molecular science. *International Journal of Molecular Sciences*, 22(3), 1–18. https://doi.org/10.3390/ijms22031467

Albisetti, G. W., Ghanem, A., Foster, E., Conzelmann, K. K., Zeilhofer, H. U., & Wildner, H. (2017). Identification of two classes of somatosensory

neurons that display resistance to retrograde infection by rabies virus. *Journal of Neuroscience*, 37(43), 10358–10371. https://doi.org/10.1523/JNEUROSCI.1277-17.2017

Andersson, L. S., Larhammar, M., Memic, F., Wootz, H., Schwochow, D., Rubin, C. J., Patra, K., Arnason, T., Wellbring, L., Hjälm, G., Imsland, F., Petersen, J. L., McCue, M. E., Mickelson, J. R., Cothran, G., Ahituv, N., Roepstorff, L., Mikko, S., Vallstedt, A., …Kullander, K. (2012). Mutations in DMRT3 affect locomotion in horses and spinal circuit function in mice. *Nature*, 488(7413), 642–646. https://doi.org/10.1038/nature11399

Antal, M., Sholomenko, G. N., Moschovakis, A. K., Storm-Mathisen, J., Heizmann, C. W., & Hunziker, W. (1992). The termination pattern and postsynaptic targets of rubrospinal fibers in the rat spinal cord: A light and electron microscopic study. *The Journal of Comparative Neurology*, 325(1), 22–37. https://doi.org/10.1002/cne.903250103

Azim, E., Jiang, J., Alstermark, B., & Jessell, T. M. (2014). Skilled reaching relies on a V2a propriospinal internal copy circuit. *Nature*, 508(7496), 357–363. https://doi.org/10.1038/nature13021

Bannatyne, B. A., Edgley, S. A., Hammar, I., Jankowska, E., & Maxwell, D. J. (2003). Networks of inhibitory and excitatory commissural interneurons mediating crossed reticulospinal actions. *European Journal of Neuroscience*, 18(8), 2273–2284. https://doi.org/10.1046/j.1460-9568.2003.02973.x

Basile, G. A., Quartu, M., Bertino, S., Serra, M. P., Boi, M., Bramanti, A., Anastasi, G. P., Milardi, D., & Cacciola, A. (2021). Red nucleus structure and function: From anatomy to clinical neurosciences. *Brain Structure and Function*, 226(1), 69–91. https://doi.org/10.1007/s00429-020-02171-x

Bodaleo, F. J., Montenegro-Venegas, C., Henríquez, D. R., Court, F. A., & Gonzalez-Billault, C. (2016). Microtubule-associated protein 1B (MAP1B)-deficient neurons show structural presynaptic deficiencies in vitro and altered presynaptic physiology. *Scientific Reports*, 6(1), 1–15. https://doi.org/10.1038/srep30069

Bowker, R. M., Westlund, K. N., Sullivan, M. C., & Coulter, J. D. (1982). Organization of descending serotonergic projections to the spinal cord. *Progress in Brain Research*, 57(C), 239–265. https://doi.org/10.1016/S0079-6123(08)64132-1

Brown, L. T. (1971). Projections and termination of the corticospinal tract in rodents. *Experimental Brain Research*, 13(4), 432–450. https://doi.org/10.1007/BF00234340

Carr, P. A., Alvarez, F. J., Leman, E. A., & Fyffe, R. E. W. (1998). Calbindin D28k expression in immunohistochemically identified Renshaw cells. *Neuroreport*, 9(11), 2657–2661. https://doi.org/10.1097/00001756-199808030-00043

Cepeda-Nieto, A. C., Pfaff, S. L., & Varela-Echavarría, A. (2005). Homeodomain transcription factors in the development of subsets of hindbrain reticulospinal neurons. *Molecular and Cellular Neuroscience*, 28(1), 30–41. https://doi.org/10.1016/j.mcn.2004.06.016

Comer, J. D., Pan, F. C., Willet, S. G., Haldipur, P., Millen, K. J., Wright, C. V. E., & Kaltschmidt, J. A. (2015). Sensory and spinal inhibitory dorsal midline crossing is independent of Robo3. *Frontiers in Neural Circuits*, 9, 36. https://doi.org/10.3389/fncir.2015.00036

Crone, S. A., Quinlan, K. A., Zagoraiou, L., Droho, S., Restrepo, C. E., Lundfald, L., Endo, T., Setlak, J., Jessell, T. M., Kiehn, O., & Sharma, K. (2008). Genetic ablation of V2a ipsilateral interneurons disrupts left-right locomotor coordination in mammalian spinal cord. *Neuron*, 60(1), 70–83. https://doi.org/10.1016/j.neuron.2008.08.009

Del Pozo, A., Manuel, R., Gonzalez, A. B. I., Koning, H. K., Habicher, J., Zhang, H., Allalou, A., Kullander, K., & Boije, H. (2020). Behavioral characterization of dmrt3a mutant zebrafish reveals crucial aspects of vertebrate locomotion through phenotypes related to acceleration. *ENeuro*, 7(3), ENEURO.0047-20.2020. https://doi.org/10.1523/ENEURO.0047-20.2020

Deng, H., Xiao, X., & Wang, Z. (2016). Periaqueductal gray neuronal activities underlie different aspects of defensive behaviors. *Journal of Neuroscience*, 36(29), 7580–7588. https://doi.org/10.1523/JNEUROSCI.4425-15.2016

Eccles, J. C., Fatt, P., & Landgren, S. (1956). Central pathway for direct inhibitory action of impulses in largest afferent nerve fibres to muscle. *Journal of Neurophysiology*, 19(1), 75–98. https://doi.org/10.1152/jn.1956.19.1.75

Eide, A. L., Glover, J., Kjaerulff, O., & Kiehn, O. (1999). Characterization of commissural interneurons in the lumbar region of the neonatal rat spinal cord. *Journal of Comparative Neurology*, 403(3), 332–345. https://doi.org/10.1002/(SICI)1096-9861(19990118)403:3<332::AID-CNE4>3.0.CO;2-R

Ericson, J., Rashbass, P., Schedl, A., Brenner-Morton, S., Kawakami, A., Van Heyningen, V., & Jessell, T. M. (1997). Pax6 controls progenitor cell identity and neuronal fate in response to graded Shh signaling concentrations of Shh are required for the induction of V1 and V2 interneurons and for MNs, with the requisite. *Cell*, 90, 169–180.

Ernfors, P., Lee, K. F., Kucera, J., & Jaenisch, R. (1994). Lack of neurotrophin-3 leads to deficiencies in the peripheral nervous system and loss of limb proprioceptive afferents. *Cell*, 77(4), 503–512. https://doi.org/10.1016/0092-8674(94)90213-5

Fitzgerald, M. (1982). The contralateral input to the dorsal horn of the spinal cord in the decerebrate spinal rat. *Brain Research*, 236(2), 275–287. https://doi.org/10.1016/0006-8993(82)90714-4

Franklin, K., & Paxinos, G. (2008). *The mouse brain in stereotaxic coordinates, compact* (3rd ed.). Academic Press. https://www.elsevier.com/books/the-mouse-brain-in-stereotaxic-coordinates-compact/franklin/978-0-12-374244-5

Gangula, P. R. R., Zhao, H., Supowit, S. C., Wimalawansa, S. J., Dipette, D. J., Westlund, K. N., Gagel, R. F., & Yallampalli, C. (2000). Increased blood pressure in α-calcitonin gene-related peptide/calcitonin gene knockout mice. *Hypertension*, 35(1 II), 470–475. https://doi.org/10.1161/01.hyp.35.1.470

Geiman, E. J., Knox, M. C., & Alvarez, F. J. (2000). Postnatal maturation of gephyrin/glycine receptor clusters on developing Renshaw cells. *The Journal of Comparative Neurology*, 426(1), 130–142. https://doi.org/10.1002/1096-9861(20001009)426:1<130::AID-CNE9>3.0.CO;2-7

Goetz, C., Pivetta, C., & Arber, S. (2015). Distinct limb and trunk premotor circuits establish laterality in the spinal cord. *Neuron*, 85(1), 131–144. https://doi.org/10.1016/j.neuron.2014.11.024

Goulding, M., Bourane, S., Garcia-Campmany, L., Dalet, A., & Koch, S. (2014). Inhibition downunder: An update from the spinal cord. In *Current opinion in neurobiology* (Vol. 26, pp. 161–166). Elsevier Ltd. https://doi.org/10.1016/j.conb.2014.03.006

Griener, A., Zhang, W., Kao, H., Haque, F., & Gosgnach, S. (2017). Anatomical and electrophysiological characterization of a population of dI6 interneurons in the neonatal mouse spinal cord. *Neuroscience*, 362, 47–59. https://doi.org/10.1016/j.neuroscience.2017.08.031

Grillner, S. (2021). The execution of movement: A spinal affair. *Journal of Neurophysiology*, 125(2), 693–698. https://doi.org/10.1152/jn.00656.2020

Holstege, G., Blok, B. F., & Ralston, D. D. (1988). Anatomical evidence for red nucleus projections to motoneuronal cell groups in the spinal cord of the monkey. *Neuroscience Letters*, 95(1–3), 97–101. https://doi.org/10.1016/0304-3940(88)90639-8

Huang, K. W., & Sabatini, B. L. (2020). Single-cell analysis of neuroinflammatory responses following intracranial injection of G-deleted rabies viruses. *Frontiers in Cellular Neuroscience*, 14, 65. https://doi.org/10.3389/fncel.2020.00065

Hultborn, H., Illert, M., & Santini, M. (1976). Convergence on interneurones mediating the reciprocal Ia inhibition of motoneurones III. Effects from supraspinal pathways. *Acta Physiologica Scandinavica*, 96(3), 368–391. https://doi.org/10.1111/j.1748-1716.1976.tb10206.x

Hultborn, H., Jankowska, E., Lindström, S., & Roberts, W. (1971). Neuronal pathway of the recurrent facilitation of motoneurones. *The Journal*

of Physiology, 218(2), 495–514. https://doi.org/10.1113/jphysiol.1971.sp009630

Iglesias González, A. B., Jakobsson, J. E. T., Vieillard, J., Lagerström, M. C., Kullander, K., & Boije, H. (2021). Single cell transcriptomic analysis of spinal Dmrt3 neurons in zebrafish and mouse identifies distinct subtypes and reveal novel subpopulations within the dI6 domain. Frontiers in Cellular Neuroscience, 15, 503. https://doi.org/10.3389/fncel.2021.781197

Jankowska, E., Bannatyne, B. A., Stecina, K., Hammar, I., Cabaj, A., & Maxwell, D. J. (2009). Commissural interneurons with input from group I and II muscle afferents in feline lumbar segments: Neurotransmitters, projections and target cells. Journal of Physiology, 587(2), 401–418. https://doi.org/10.1113/jphysiol.2008.159236

Kawatani, M., de Groat, W. C., Itoi, K., Uchida, K., Sakimura, K., Yamanaka, A., Yamashita, T., & Kawatani, M. (2021). Downstream projection of Barrington's nucleus to the spinal cord in mice. Journal of Neurophysiology, 126(6), 1959–1977. https://doi.org/10.1152/jn.00026.2021

Kim, E. J., Jacobs, M. W., Ito-Cole, T., & Callaway, E. M. (2016). Improved monosynaptic neural circuit tracing using engineered rabies virus glycoproteins. Cell Reports, 15(4), 692–699. https://doi.org/10.1016/j.celrep.2016.03.067

Kishore, S., Cadoff, E. B., Agha, M. A., & McLean, D. L. (2020). Orderly compartmental mapping of premotor inhibition in the developing zebrafish spinal cord. Science, 370(6515), 431–436. https://doi.org/10.1126/science.abb4608

Klein, R., Silos-Santiago, I., Smeyne, R. J., Lira, S. A., Brambilla, R., Bryant, S., Zhang, L., Snider, W. D., & Barbacid, M. (1994). Disruption of the neurotrophin-3 receptor gene trkC eliminates Ia muscle afferents and results in abnormal movements. Nature, 368(6468), 249–251. https://doi.org/10.1038/368249a0

Koch, S. C. (2019). Motor task-selective spinal sensorimotor interneurons in mammalian circuits. In Current opinion in physiology (Vol. 8, pp. 129–135). Elsevier Ltd. https://doi.org/10.1016/j.cophys.2019.01.014

Krashes, M. J., Koda, S., Ye, C. P., Rogan, S. C., Adams, A. C., Cusher, D. S., Maratos-Flier, E., Roth, B. L., & Lowell, B. B. (2011). Rapid, reversible activation of AgRP neurons drives feeding behavior in mice. Journal of Clinical Investigation, 121(4), 1424–1428. https://doi.org/10.1172/JCI46229

Küchler, M., Fouad, K., Weinmann, O., Schwab, M. E., & Raineteau, O. (2002). Red nucleus projections to distinct motor neuron pools in the rat spinal cord. Journal of Comparative Neurology, 448(4), 349–359. https://doi.org/10.1002/cne.10259

Lavin, T. K., Jin, L., Lea, N. E., & Wickersham, I. R. (2020). Monosynaptic tracing success depends critically on helper virus concentrations. Frontiers in Synaptic Neuroscience, 12, 6. https://doi.org/10.3389/fnsyn.2020.00006

Lein, E. S., Hawrylycz, M. J., Ao, N., Ayres, M., Bensinger, A., Bernard, A., Boe, A. F., Boguski, M. S., Brockway, K. S., Byrnes, E. J., Chen, L., Chen, L., Chen, T. M., Chin, M. C., Chong, J., Crook, B. E., Czaplinska, A., Dang, C. N., Datta, S., … Jones, A. R. (2007). Genome-wide atlas of gene expression in the adult mouse brain. Nature, 445(7124), 168–176. https://doi.org/10.1038/nature05453

Liang, H., Paxinos, G., & Watson, C. (2012). The red nucleus and the rubrospinal projection in the mouse. Brain Structure and Function, 217(2), 221–232. https://doi.org/10.1007/s00429-011-0348-3

Liang, H., Watson, C., & Paxinos, G. (2015). Projections from the oral pontine reticular nucleus to the spinal cord of the mouse. Neuroscience Letters, 584, 113–118. https://doi.org/10.1016/j.neulet.2014.10.025

Liang, H., Watson, C., & Paxinos, G. (2016). Terminations of reticulospinal fibers originating from the gigantocellular reticular formation in the mouse spinal cord. Brain Structure and Function, 221(3), 1623–1633. https://doi.org/10.1007/s00429-015-0993-z

Lu, D. C., Niu, T., & Alaynick, W. A. (2015). Molecular and cellular development of spinal cord locomotor circuitry. Frontiers in Molecular Neuroscience, 8, 25. https://doi.org/10.3389/fnmol.2015.00025

Lundfald, L., Restrepo, C. E., Butt, S. J. B., Peng, C. Y., Droho, S., Endo, T., Zeilhofer, H. U., Sharma, K., & Kiehn, O. (2007). Phenotype of V2-derived interneurons and their relationship to the axon guidance molecule

EphA4 in the developing mouse spinal cord. European Journal of Neuroscience, 26(11), 2989–3002. https://doi.org/10.1111/j.1460-9568.2007.05906.x

Madisen, L., Zwingman, T. A., Sunkin, S. M., Oh, S. W., Zariwala, H. A., Gu, H., Ng, L. L., Palmiter, R. D., Hawrylycz, M. J., Jones, A. R., Lein, E. S., & Zeng, H. (2010). A robust and high-throughput Cre reporting and characterization system for the whole mouse brain. Nature Neuroscience, 13(1), 133–140. https://doi.org/10.1038/nn.2467

Malmberg, A. B., Chen, C., Tonegawa, S., & Basbaum, A. I. (1997). Preserved acute pain and reduced neuropathic pain in mice lacking PKCγ. Science, 278(5336), 279–283.

Mendes-Gomes, J., Motta, S. C., Passoni Bindi, R., de Oliveira, A. R., Ullah, F., Baldo, M. V. C., Coimbra, N. C., Canteras, N. S., & Blanchard, D. C. (2020). Defensive behaviors and brain regional activation changes in rats confronting a snake. Behavioural Brain Research, 381, 112469. https://doi.org/10.1016/j.bbr.2020.112469

Mihailoff, G. A., & Haines, D. E. (2017). Motor system I: Peripheral sensory, brainstem, and spinal influence on anterior horn neurons. In Fundamental neuroscience for basic and clinical applications (5th ed., pp. 346–359. e1). Elsevier Inc. https://doi.org/10.1016/B978-0-323-39632-5.00024-4

Misgeld, T., Burgess, R. W., Lewis, R. M., Cunningham, J. M., Lichtman, J. W., & Sanes, J. R. (2002). Roles of neurotransmitter in synapse formation: Development of neuromuscular junctions lacking choline acetyltransferase. Neuron, 36(4), 635–648. https://doi.org/10.1016/S0896-6273(02)01020-6

Noga, B. R., Johnson, D. M. G., Riesgo, M. I., & Pinzon, A. (2009). Locomotor-activated neurons of the Cat. I. Serotonergic innervation and co-localization of 5-HT$_7$, 5-HT$_{2A}$, and 5-HT$_{1A}$ receptors in the thoracolumbar spinal cord. Journal of Neurophysiology, 102(3), 1560–1576. https://doi.org/10.1152/jn.91179.2008

Nudo, R. J., & Masterton, R. B. (1988). Descending pathways to the spinal cord: A comparative study of 22 mammals. Journal of Comparative Neurology, 277(1), 53–79. https://doi.org/10.1002/cne.902770105

Nyberg-Hansen, R. (1966). Functional organization of descending supraspinal fibre systems to the spinal cord. Anatomical observations and physiological correlations. Ergebnisse Der Anatomie Und Entwicklungsgeschichte, 39(2), 3–48. https://pubmed.ncbi.nlm.nih.gov/5959914/

Nyberg-Hansen, R., & Brodal, A. (1964). Sites and mode of termination of rubrospinal fibres in the cat. An experimental study with silver impregnation methods. Journal of Anatomy, 98(Pt 2), 235–253. https://www.ncbi.nlm.nih.gov/pmc/articles/PMC1261279/

Osakada, F., Mori, T., Cetin, A. H., Marshel, J. H., Virgen, B., & Callaway, E. M. (2011). New rabies virus variants for monitoring and manipulating activity and gene expression in defined neural circuits. Neuron, 71(4), 617–631. https://doi.org/10.1016/j.neuron.2011.07.005

Patiño, M., Lagos, W. N., Patne, N. S., Tasic, B., Zeng, H., & Callaway, E. M. (2022). Single-cell transcriptomic classification of rabies-infected cortical neurons. Proceedings of the National Academy of Sciences, 119(22), e2203677119. https://doi.org/10.1073/pnas.2203677119

Perry, S., Larhammar, M., Vieillard, J., Nagaraja, C., Hilscher, M. M., Tafreshiha, A., Rofo, F., Caixeta, F. V., & Kullander, K. (2019). Characterization of Dmrt3-derived neurons suggest a role within locomotor circuits. Journal of Neuroscience, 39(10), 1771–1782. https://doi.org/10.1523/JNEUROSCI.0326-18.2018

Pimpinella, S., & Zampieri, N. (2022). Rabies anterograde monosynaptic tracing reveals organization of spinal sensory circuits. Neuroscience, 491, 75–86. https://doi.org/10.1016/j.neuroscience.2022.03.011

Preibisch, S., Saalfeld, S., & Tomancak, P. (2009). Globally optimal stitching of tiled 3D microscopic image acquisitions. Bioinformatics, 25(11), 1463–1465. https://doi.org/10.1093/bioinformatics/btp184

Prosniak, M., Hooper, D. C., Dietzschold, B., & Koprowski, H. (2001). Effect of rabies virus infection on gene expression in mouse brain. Proceedings of the National Academy of Sciences of the United States of America, 98(5), 2758–2763. https://doi.org/10.1073/pnas.051630298

Satou, C., Sugioka, T., Uemura, Y., Shimazaki, T., Zmarz, P., Kimura, Y., & Higashijima, S. I. (2020). Functional diversity of glycinergic commissural inhibitory neurons in larval zebrafish. *Cell Reports*, *30*(9), 3036–3050. e4. https://doi.org/10.1016/j.celrep.2020.02.015

Schneider, C. A., Rasband, W. S., & Eliceiri, K. W. (2012). NIH Image to ImageJ: 25 years of image analysis. *Nature Methods*, *9*(7), 671–675. https://doi.org/10.1038/nmeth.2089

Schnerwitzki, D., Perry, S., Ivanova, A., Caixeta, F. V., Cramer, P., Günther, S., Weber, K., Tafreshiha, A., Becker, L., Vargas Panesso, I. L., Klopstock, T., Hrabe de Angelis, M., Schmidt, M., Kullander, K., & Englert, C. (2018). Neuron-specific inactivation of Wt1 alters locomotion in mice and changes interneuron composition in the spinal cord. *Life Science Alliance*, *1*(4), e201800106. https://doi.org/10.26508/lsa.201800106

Stachowski, N. J., & Dougherty, K. J. (2021). Review spinal inhibitory interneurons: Gatekeepers of sensorimotor pathways. *International Journal of Molecular Sciences*, *22*(5), 1–17. https://doi.org/10.3390/ijms22052667

Sun, S., Xu, Q., Guo, C., Guan, Y., Liu, Q., & Dong, X. (2017). Leaky gate model: Intensity-dependent coding of pain and itch in the spinal cord. *Neuron*, *93*(4), 840–853. e5. https://doi.org/10.1016/j.neuron.2017.01.012

Tracey, D. (2004). Ascending and descending pathways in the spinal cord. In *The rat nervous system* (pp. 149–164). Elsevier Inc. https://doi.org/10.1016/B978-012547638-6/50008-0

ten Donkelaar, H. J., & de Boer-van Huizen, R. (1982). Observations on the development of descending pathways from the brain stem to the spinal cord in the clawed toad *Xenopus laevis. Anatomy and Embryology*, *163*(4), 461–73. https://doi.org/10.1007/BF00305559

Tsetsenis, T., Badyna, J. K., Wilson, J. A., Zhang, X., Krizman, E. N., Subramaniyan, M., Yang, K., Thomas, S. A., & Dani, J. A. (2021). Midbrain dopaminergic innervation of the hippocampus is sufficient to modulate formation of aversive memories. *Proceedings of the National Academy of Sciences of the United States of America*, *118*(40), e2111069118. https://doi.org/10.1073/pnas.2111069118

Ueno, M., Nakamura, Y., Li, J., Gu, Z., Niehaus, J., Maezawa, M., Crone, S. A., Goulding, M., Baccei, M. L., & Yoshida, Y. (2018). Corticospinal circuits from the sensory and motor cortices differentially regulate skilled movements through distinct spinal interneurons. *Cell Reports*, *23*(5), 1286–1300. e7. https://doi.org/10.1016/j.celrep.2018.03.137

Usoskin, D., Furlan, A., Islam, S., Abdo, H., Lönnerberg, P., Lou, D., Hjerling-Leffler, J., Haeggström, J., Kharchenko, O., Kharchenko, P. V., Linnarsson, S., & Ernfors, P. (2015). Unbiased classification of sensory neuron types by large-scale single-cell RNA sequencing. *Nature Neuroscience*, *18*(1), 145–153. https://doi.org/10.1038/nn.3881

Verstegen, A. M. J., Vanderhorst, V., Gray, P. A., Zeidel, M. L., & Geerling, J. C. (2017). Barrington's nucleus: Neuroanatomic landscape of the mouse "pontine micturition center". *Journal of Comparative Neurology*, *525*(10), 2287–2309. https://doi.org/10.1002/cne.24215

Wall, N. R., Wickersham, I. R., Cetin, A., De La Parra, M., & Callaway, E. M. (2010). Monosynaptic circuit tracing in vivo through Cre-dependent targeting and complementation of modified rabies virus. *Proceedings of the National Academy of Sciences of the United States of America*, *107*(50), 21848–21853. https://doi.org/10.1073/pnas.1011756107

Wang, Z., Chabot, J. G., & Quirion, R. (2011). On the possible role of ERK, p38 and CaMKII in the regulation of CGRP expression in morphine-tolerant rats. *Molecular Pain*, *7*, 1744-8069-7–68. https://doi.org/10.1186/1744-8069-7-68

Wang, Z., Maunze, B., Wang, Y., Tsoulfas, P., & Blackmore, M. G. (2018). Global connectivity and function of descending spinal input revealed by 3D microscopy and retrograde transduction. *Journal of Neuroscience*, *38*(49), 10566–10581. https://doi.org/10.1523/JNEUROSCI.1196-18.2018

Wang, Z., Romanski, A., Mehra, V., Wang, Y., Campbell, B. C., Petsko, G. A., Tsoulfas, P., & Blackmore, M. (2021). Brain-wide analysis of the supraspinal connectome reveals anatomical correlates to functional recovery after spinal injury. BioRxiv. 2021.06.10.447885. https://doi.org/10.1101/2021.06.10.447885

Warner, G., & Watson, C. R. R. (1972). The rubrospinal tract in a diprotodont marsupial (*Trichosurus vulpecula*). *Brain Research*, *41*(1), 180–183. https://doi.org/10.1016/0006-8993(72)90625-7

Watson, C., & Harrison, M. (2012). The location of the major ascending and descending spinal cord tracts in all spinal cord segments in the mouse: Actual and extrapolated. *The Anatomical Record: Advances in Integrative Anatomy and Evolutionary Biology*, *295*(10), 1692–1697. https://doi.org/10.1002/ar.22549

Watson, C., Paxinos, G., Kayalioglu, G., & Heise, C. (2009). Atlas of the mouse spinal cord. In *The spinal cord* (pp. 308–379). Elsevier Ltd. https://doi.org/10.1016/B978-0-12-374247-6.50020-1

Watson, C., Paxinos, W., & Luis, P. (2011). *The mouse nervous system* (1st ed.). Academic Press. https://www.elsevier.com/books/the-mouse-nervous-system/watson/978-0-12-369497-3

Wild, J. M., Cabot, J. B., Cohen, D. H., & Karten, H. J. (1979). Origin, course and terminations of the rubrospinal tract in the pigeon (*Columba livia*). *The Journal of Comparative Neurology*, *187*(4), 639–654. https://doi.org/10.1002/cne.901870402

Wu, H., Petitpré, C., Fontanet, P., Sharma, A., Bellardita, C., Quadros, R. M., Jannig, P. R., Wang, Y., Heimel, J. A., Cheung, K. K. Y., Wanderoy, S., Xuan, Y., Meletis, K., Ruas, J., Gurumurthy, C. B., Kiehn, O., Hadjab, S., & Lallemend, F. (2021). Distinct subtypes of proprioceptive dorsal root ganglion neurons regulate adaptive proprioception in mice. *Nature Communications*, *12*(1), 1–13. https://doi.org/10.1038/s41467-021-21173-9

Yuan, A., Sershen, H., Veeranna, B., B, S., Kumar, A., Hashim, A., Berg, M., Lee, J. H., Sato, Y., Rao, M. V., Mohan, P. S., Dyakin, V., Julien, J. P., Lee, V. M. Y., & Nixon, R. A. (2015). Neurofilament subunits are integral components of synapses and modulate neurotransmission and behavior in vivo. *Molecular Psychiatry*, *20*(8), 986–994. https://doi.org/10.1038/mp.2015.45

Zagoraiou, L., Akay, T., Martin, J. F., Brownstone, R. M., Jessell, T. M., & Miles, G. B. (2009). A cluster of cholinergic premotor interneurons modulates mouse locomotor activity. *Neuron*, *64*(5), 645–662. https://doi.org/10.1016/j.neuron.2009.10.017

Zampieri, N., Jessell, T. M., & Murray, A. J. (2014). Mapping sensory circuits by anterograde transsynaptic transfer of recombinant rabies virus. *Neuron*, *81*(4), 766–778. https://doi.org/10.1016/j.neuron.2013.12.033

Zhang, J., Lanuza, G. M., Britz, O., Wang, Z., Siembab, V. C., Zhang, Y., Velasquez, T., Alvarez, F. J., Frank, E., & Goulding, M. (2014). V1 and V2b interneurons secure the alternating flexor-extensor motor activity mice require for limbed locomotion. *Neuron*, *82*(1), 138–150. https://doi.org/10.1016/j.neuron.2014.02.013

Zheng, Y., Liu, P., Bai, L., Trimmer, J. S., Bean, B. P., & Ginty, D. D. (2019). Deep sequencing of somatosensory neurons reveals molecular determinants of intrinsic physiological properties. *Neuron*, *103*(4), 598–616. e7. https://doi.org/10.1016/j.neuron.2019.05.039

SUPPORTING INFORMATION

Additional supporting information can be found online in the Supporting Information section at the end of this article.

How to cite this article: Vieillard, J., Franck, M. C. M., Hartung, S., Jakobsson, J. E. T., Ceder, M. M., Welsh, R. E., Lagerström, M. C., & Kullander, K. (2023). Adult spinal Dmrt3 neurons receive direct somatosensory inputs from ipsi- and contralateral primary afferents and from brainstem motor nuclei. *Journal of Comparative Neurology*, *531*, 5–24. https://doi.org/10.1002/cne.25405